5-2014

# HYDROTHERMAL SYNTHESIS OF ORGANICALLY-LINKED POLYOXOMETALATES

Riyadh Alshammari
*Clemson University*, riyadh1@live.com

# HYDROTHERMAL SYNTHESIS OF ORGANICALLY-LINKED POLYOXOMETALATES

---

A Thesis
Presented to
the Graduate School of
Clemson University

---

In Partial Fulfillment
of the Requirements for the Degree
Master of Science
Chemistry

---

by
Riyadh Hamdan Alshammari
May 2014

---

Accepted by:
Dr. Shiou-Jyh Hwu, Committee Chair
Dr. Daniel Whitehead
Dr. Andrew Tennyson

## ABSTRACT

In the last two decades, the research in the field of polyoxometalates (POMs) has flourished dramatically due to the fascinating applications of these novel materials ranging from catalysis, medicine, electrochemistry, photochromism, to magnetism. POMs are aggregates of transition metal-oxide anions linked thorough covalent bonding. The work presented in this thesis focuses on the synthesis and structural characterization of new POM-containing structures as well as the study of parameters that led to the optimal conditions for the synthesis of the herein described compounds.

In the first chapter, POM based inorganic-organic hybrid system will be discussed. The structure of $(H_2bpy)(Hbpy)_2(V_{15}O_{36}Cl)\cdot n(H_2O)$ have been synthesized by hydrothermal method in acidic solution at 160 $^oC$. This new phase exhibits extended 2D structure featuring non-covalent bonding; π-π stacking, hydrogen bonding and anion- π interaction. The POM clusters are linked through by organic molecule (4,4'-bipyridine) via hydrogen bonding. The linkage between POMs and organic molecules by the means of hydrogen bonding is extremely rare and the work in this thesis presents an opportunity to shine some light on the synthetic approaches and conditions under which these materials form. $Cs_2Mn_4(S_2O_7)(SO_4)_2$ - a chain-like structure - and other newly synthesized POM compound with the composition of $Cs_4(SO_4@V_{12}As_8O_{40})$ have been presented in the second chapter.

Some characterization techniques used to identify and confirm the content of new phases such as single X-ray diffraction, Powder X-ray diffraction, Energy-dispersive X-ray spectroscopy (EDX) and Scanning electron microscope (SEM) were used. Also, IR and Thermogravimetric analysis (TGA) have been used throughout the study for selected compounds.

# DEDICATION

I would like to dedicate this work to my family here in the USA and back home overseas. Without their support, love and encouragement, this work would not have been done.

# ACKNOWLEDGMENTS

I would like to sincerely thank my research advisor, Dr. Shiou-Jyh Hwu for his guidance and support throughout my graduate studies and for providing me with all the resources necessary to be successful in this effort. I would also like to thank Dr. Daniel Whitehead and Dr. Andrew Tennyson for serving as my committee members.

I wish to express my appreciation to the Hwu Research Group past members, Dr. Palmer West, Dr. Duminda Sanjeewa and present members Dr. Jianhua Gao, Justin Talbert and Kathryn Perkins. I would like to especially thank Dino Sulejmanovic for his willingness to help and train me, and his assistance solving problems and support throughout my study.

Also I am thankful to the government of the Kingdom of Saudi Arabia and King Saud University for giving me the chance to pursue my graduate study and providing me with generous scholarship to complete my Master degree in the United States of America.

Most importantly, I want to thank God, who blesses me with everything. “And whatever you have of favor - it is from Allah, God.” [Qur’an 16:53]

TABLE OF CONTENTS

Page

Table of Contents (Continued)

Page

LIST OF TABLES

List of Tables (Continued)

Table Page

LIST OF FIGURES

List of Figures (Continued)

Figure Page

# CHAPTER ONE

# INTRODUCTION

Solid state chemistry is a branch of solid state science that studies solid materials with respect to their synthesis, structure, properties and applications. Solids that are molecular and nonmolecular can be either crystalline or noncrystalline. Molecular solids are made of covalently bonded molecules that are held together by weak forces such as H-bonding, dipole-dipole and induced-dipole, and van der Waals forces. As a result of weak interactions, molecular solids are often considered soft materials due to low melting (or decomposition) temperatures. Non-molecular solids have extended structures made of extended arrays of atoms and their properties are determined by how the atoms are packed in three dimensions (3D). The bonding between atoms in extended solids is made of mostly covalent and ionic interactions which are much stronger compared with those of molecular solids. Consequently, extended solids tend to have high melting points and exhibit unique transport properties, *e.g.*, superconductivity due to itinerant (delocalized) electrons. Therefore, in order to understand the properties of solid materials it is important to understand the structure of solids and the nature of bond interactions.[1]

Since the discovery of X-ray crystallography in the early 1900's by William Lawrence Bragg, the field of solid state chemistry has been expanded dramatically due to the improved characterization of newly synthesized materials. The field of solid state chemistry has been driven by the materials applications of technological importance, such as ferroelectric perovskites discovered in the 1940's[2], zeolite and platinum-based catalysts in the 1950's[3], *LASER* of Nd:YAG in the 1960's [4], high *T*c superconductors in

the 1980's[5], and the colossal magnetoresistant manganese perovskites in the 1990' s [6], to just name a few. Currently, the global demand for alternative energy sources has led to research in solid state materials for applications and devices such as hydrogen storage[7], solar cells[8], fuel cells[9], and lithium batteries.[10] With much improved characterization techniques using X-ray diffraction, in particular, our fundamental understanding of structure and bonding that govern the physical properties of new materials have been advanced, thus new initiatives of advanced materials research have emerged.

One of the thrust areas of our research deals with exploratory synthesis of new inorganic-organic hybrid materials for energy storage. It is well-known that relevant to the research described later in this thesis, inorganic-organic hybrid solids studied thus far are largely made of coordination complexes where the organic molecules are acting like a ligand to coordinate around metal cations. In this research, we will employ polyoxometalate (POM) anions as an inorganic building block to replace otherwise oppositely charged metal cations in hopes to synthesize extended hybrid frameworks with rich redox chemistry. POM clusters are made of aggregates of transition-metal (TM) oxide units and can be employed as a charge reservoir during multi-electron chemical reactions involving multiple TM cations. These inorganic clusters possess an unmatched range of physical (such as magnetism) and chemical properties, acting as a set of transferable building blocks that can reliably be utilized in the formation of new materials with desired functionalities associated with versatile electronic structures.[15,16] One of the challenges is of course to imagine how these anionic clusters could interact with organic molecules that are necessary for the formation of new hybrids. We anticipate, therefore,

that the "coordination" chemistry between POM anions and organic molecules is going to be different than that observed in the conventional hybrids based on metal cations. This thesis study will take an initial step to explore this new chemistry and to illustrate the structure and bonding of resulting solids for our continued research development in POM-based hybrids.

The major focus of my study is about the synthesis and characterization of new extended solids made of, more specifically, polyoxovanadate (POV) and 4,4'-bipyridine (bpy) organic molecules through self-assembly. Our primary course of investigation is concerning the bonding at the interface of these two chemically dissimilar chemicals and the optimal reaction conditions upon which the self-assembly takes place. In this thesis, the new structures containing POV clusters will be discussed. The optimal synthetic conditions will be illustrated in conjunction with the discovery of new compounds through both successful and unsuccessful reactions which feature "transformations" and decompositions of employed POV cluster starting material. A newly discovered hybrid solid, $(H_2bpy)(Hbpy)_2(V_{15}O_{36}Cl)\cdot n(H_2O)$, was synthesized by employing water-soluble polyoxovanadate salt $Cs_5V_{14}As_8O_{42}Cl$ as a precursor. The reaction took placed in an acidic solution of mixed water and ethanol at 160 $^oC$. Using the same precursor, two other new compounds, $Cs_4(SO_4@V_{12}As_8O_{40})$ and $Cs_2Mn_4(S_2O_7)(SO_4)_2$ were isolated from reactions under different conditions.

Prior to this study, a new POV-bpy hybrid was discovered by Brett Hester, a former undergraduate researcher, and Mr. Dino Sulejmanovic, a graduate student of the research group.[23] Tentatively, its structural composition is $(H_2byp)_2(Cl@V_{14}As_8O_{42}Cl)$ as

suggested by the single crystal X-ray diffraction studies. The single crystals were grown under hydrothermal conditions using $Cs_5V_{14}As_8O_{42}Cl$, $ZnCl_2$, 4,4'-bipyridine in 1:1:10 mol ratios, respectively. The yield of the single crystals was estimated qualitatively to be about 60% of the overall filtered product. The structure, as shown in Fig. 1.1, indicates the incorporation of the employed POV cluster, $\{Cl@V_{14}As_8O_{42}Cl\}$, and the extended structure is constructed through the H-bonding interaction between POV anion and protonated 4,4'-bipyridine.

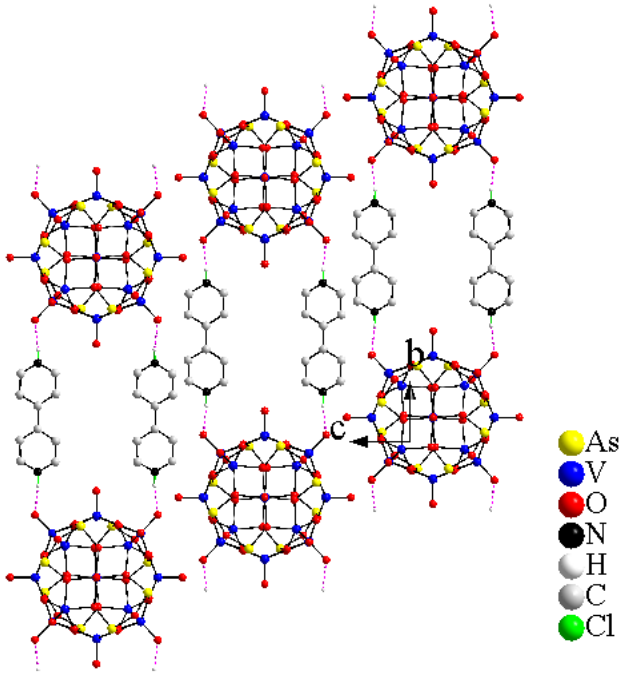


Figure 1.1: Partial structure of $(H_2byp)_2(Cl@V_{14}As_8O_{42}Cl)$ showing the connectivity between the $\{Cl@V_{14}As_8O_{42}Cl\}$ cluster and protonated 4,4'-bipyridine molecules.

Before discussing the results of my thesis study, I will give some background information in the following paragraphs about polyoxometalates in terms of the definition and the history of some selected compounds along with their applications.

## Polyoxometalates

Polyoxometalates (POMs), as mentioned above, are aggregates of metal-oxide units based on transition metals, which are typically V, Mo, W and Nb. These metal cations are in their high oxidation states, linked together by shared oxygen atoms to form clusters with finite size and geometry. Besides the metal oxide units, POM clusters can also encapsulate heteroatoms such as P, Si, As and S. The first POM compound which was identified by X-ray crystallography was $[PMo_{12}O_{40}]^{3-}$ in 1928 by J.F. Keggin. Since that time, the term "Keggin structure" has been used to describe any structure with the general formula $(XM_xO_{40})^{n-}$, where x is typically 12 but can also be lower and n is the negative charge.[24] POMs have remarkable properties and a great deal of potential to meet demands of multiple fields regarding health, environment, energy and information technologies.[11] The research regarding POM chemistry received tremendous impetus from the incisive review by Pope and Muller in 1991 and has accordingly witnessed considerable progress in the last two decades.[12-13]

POMs possess many attractive properties; generally, they exhibit extended thermal and oxidative stabilities. These structurally confined clusters, due to their structural analogy with metal oxides regarding their metal coordination and connectivity,

they are considered as (soluble) molecular oxides. Moreover, POMs show rich redox characteristics that make them conceivably good electron/charge reservoirs.[12]

POMs exist in a large variety of structure compositions which can be divided into two major families; first, the isopoly compounds, or isopolyoxometalates, that contain only the d-block metal cations interlinked through oxide anions. The second type is the heteropolyoxometalates compounds that contain one or more p-, d-, or f-block "heteroatoms" in addition to the ions involved in the formation of metal-oxide cluster. Figure 1.2 illustrates some of the representative POM structures discovered thus far.[14]

The formation of a specific POM type is controlled by a relatively long list of experimental variables, which are often considered by researchers when targeting the synthesis of a given polyoxometalate archetype from bottom-up approaches. These variables, include, but are not limited to: [15-16]

- concentration/type of metal oxide anion
- acidity of the solution (pH)
- ionic strength
- heteroatom type/concentration,
- presence of additional ligands
- reducing environment,
- temperature and pressure of reaction (e.g. microwave, hydrothermal, refluxing)
- counter-ion and metal-ion effect

Variation of these parameters apparently allows for a large variety of POM structures to be formed, and in turn a versatile library of linkable units for structures of desired

frameworks to form. Isopolyoxometalates can be transformed to heteropolyoxometalates by encapsulating heteroatoms at the optimal conditions of acidity and temperature.

Unpaired electrons in the reduced POM clusters can be delocalized.[16] These clusters are formally composed of localized magnetic moments that can undergo a rapid hopping (exchange) over the magnetic sites.[20] In fact, when magnetic ions are brought within a close proximity, magnetic exchange can occur. The $O^{2-}$ bonds tend to be more covalent in character and can promote magnetic exchange. The electron density within the cluster is delocalized, therefore, showing mixed valence sites. [21, 22]

Inspired by metal-organic framework (MOF) materials, a new area of research, so called polyoxometalate-organic-frameworks (POMOFs), has been emerged. POMOFs, also called POM-based inorganic-organic hybrids result from the combination of POMs as building blocks and organic/metal species as linkers.[17,18] Three main linkage modes of POMOFs have been observed as shown in Figure 1.1 a-c. These modes can be described as coordination networks made of i) organic units linking POMs and metal ions (Figure 1.1(a)) through which most of the POMOF open-framework solids are constructed, ii) transition metal cations coupling directly to terminal oxygen atoms of POMs (Figure 1.1(b)), and iii) like i), organic units linking to POMs through transition metal cations instead (Figure 1.1(c)).[17] The work presented in this thesis suggests a relatively rare mode, to the best of our knowledge, of linkage in POM-based inorganic-organic hybrid materials. The structure discussed in the first chapter in fact shows a connection between POMs and organic molecules through unconventional bonding, as highlighted in Figure 1.1(d).

The discussion of this thesis is, in chapter two, primarily focuses on the bonding between atoms and the thermal properties of the hydrothermally synthesized ($T < 200\ ^{o}C$) POV-organic compound as well as how the synthetic conditions entice self-assembly and thermal properties. In chapter three, we have discussed structures of two new compounds that were isolated in the failed reactions which were designed to seek optimal reaction conditions for self-assembly of inorganic-organic hybrids discussed in second chapter. In the conclusion chapter, chapter four, we offer some comments about critical parameters that govern the formation of POM-organic self-assembly in terms of reaction conditions and bonding interactions for future studies.

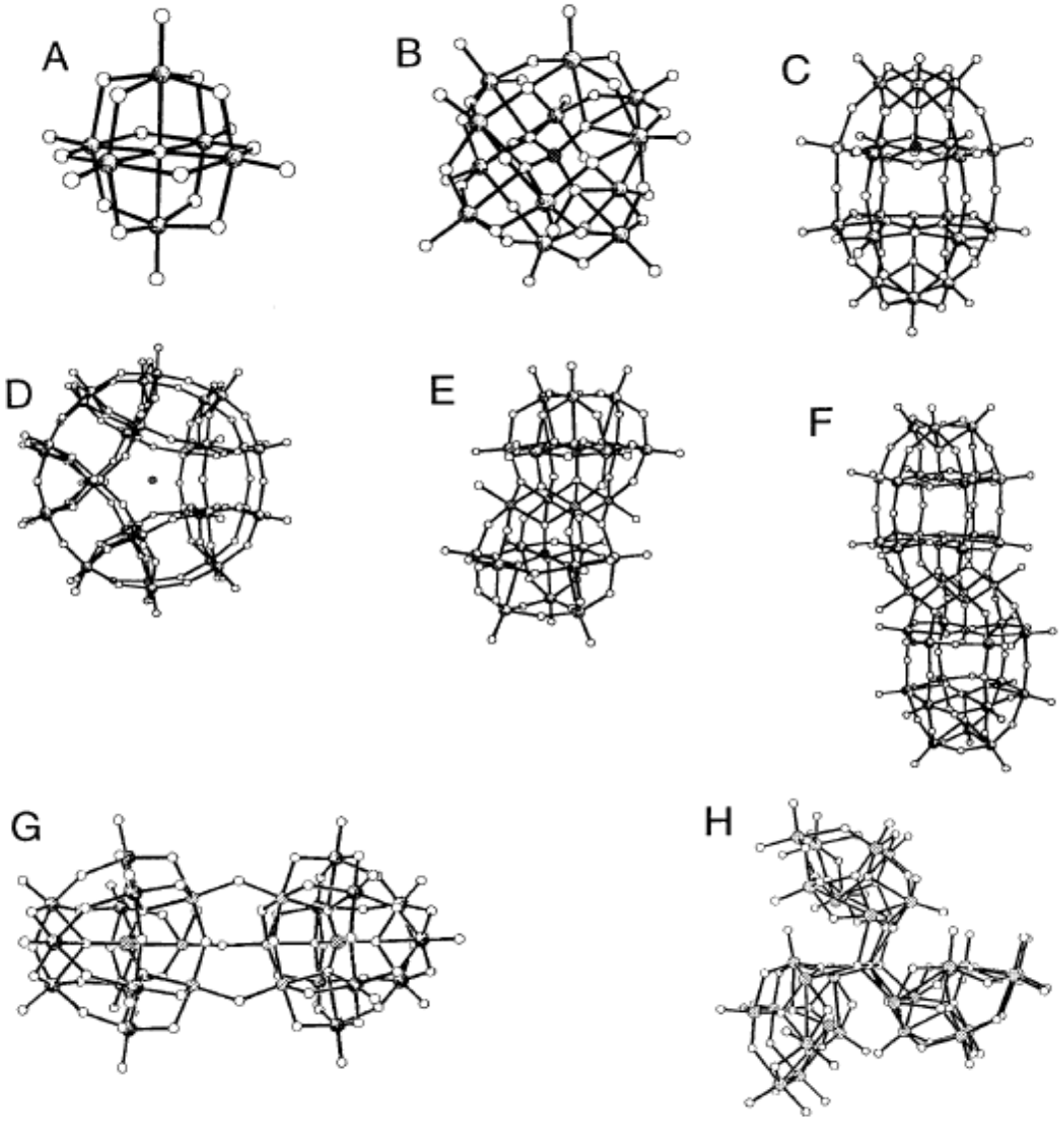


Figure 1.2: Atom notation ("ball-and-stick") drawings of 8 representative structural families of POMs: **(A)** the hexametalate structure, $[M_6O_{19}]^{x-}$; **(B)** common Keggin structure, $[XW_{12}O_{40}]^{x-}$ ; **(C)** the Wells-Dawson structure, $[X_2W_{18}O_{62}]^{x-}$ ; **(D)** the Pope-Jeannin-Preyssler (PJP) structure, $[MP_5W_{30}O_{110}]^{x-}$ ; **(E)** the trivacant Keggin-derived sandwich complex, $[(M^{II})_2(M^{II}L)_2(PW_9O_{34})_2]^{10-}$; **(F)** the trivacant Wells-Dawson-derived sandwich complex, $[(M^{II})_2(M^{II}L)_2(P_2W_{15}O_{56})_2]^{16-}$; **(G)** the double-Keggin structure, $[\{A\text{-}R\text{-}SiO_4W_9O_{30}(OH)_3M_3\}_2(OH)_3]^{11-}$; and **(H)** HPA-23, $[NaSb_9W_{21}O_{86}]^{18-}$. Atom designations: O ) open circle; W ) dotted; heteroatoms ) parallel lines or crossed hatched. [Adopted from reference 14, Rhule, J.; Hill, C.; Judd, D.; Schinazi, R.; *Chemical Reviews*, **1998**, *98*, 327-357 . Copyright 1998 American Chemical Society]

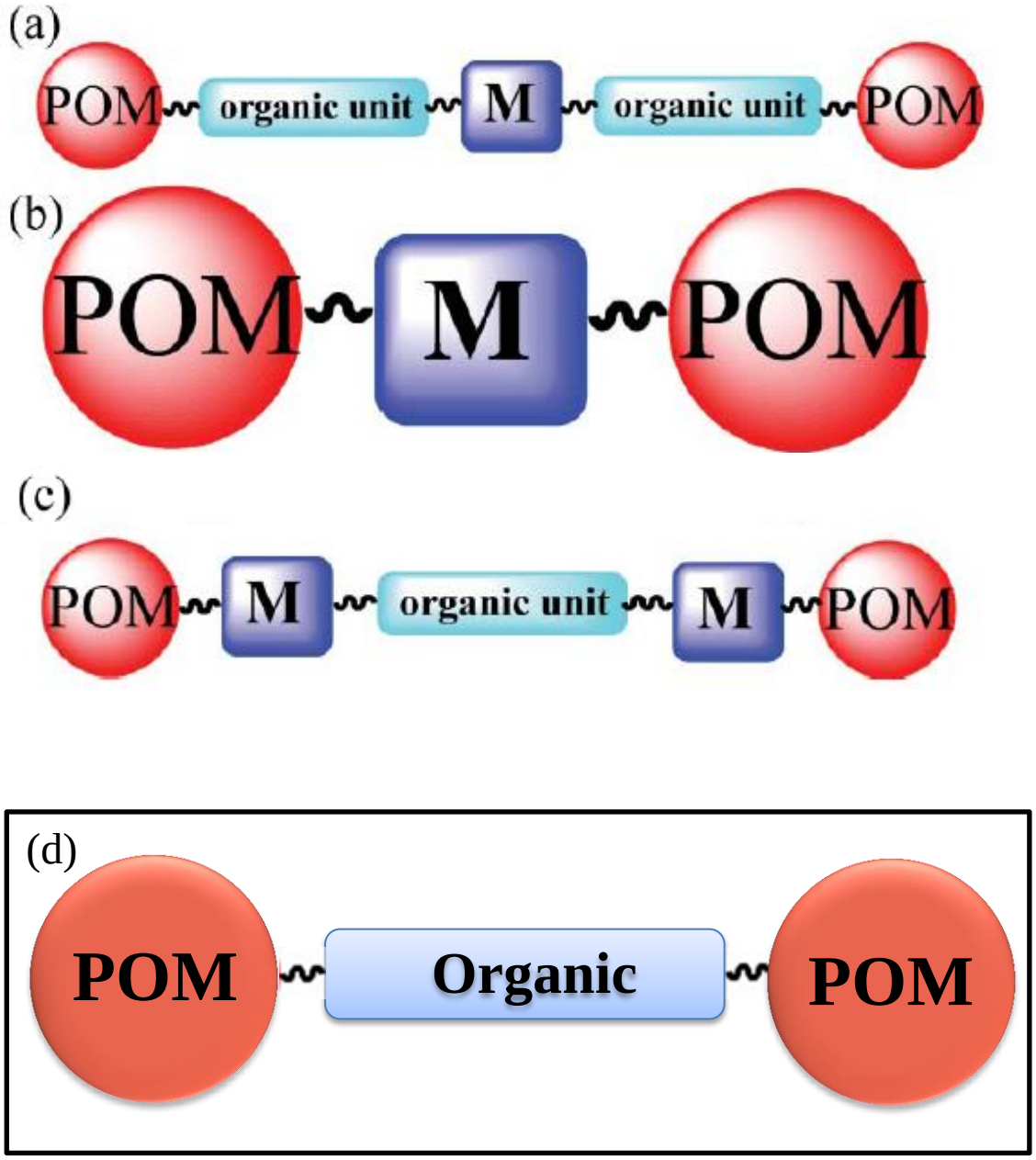


Figure 1.3(a-c)**:** Schematic representation of the three major ways to link POMs. M: transition metal ions [adopted from ref 19, Wang,Y.; Ye,L.; Wang, T.; Cui, X.; Shi, S.; Wanga, S.; Xu, J.; *Dalton Trans*., **2010**, 39, 1916–1919, Copyright 2010 The Royal Society of Chemistry]. (**d**) a newly proposed mode through self-assembly of POM and organic unit.

Literature Cited


1. West, A. R. *Solid State Chemistry and Its Applications*; John Wiley & Sons: NewYork, 1996.

2. Cross, L. E.; Newnham, R. E. *Ceramics and Civilization*, Vol. III, ed. Kingery, W. D., The American Ceramic Society Inc.: Ohio, **1987**, 289–291.

3. Rabo, J. A.; Schoonover, M. W. *Appl. Catal. A: Gen.* **2001**, *222*, 261–275.

4. Geusic, J. E.; Marcos, H. M.; van Uitert, L. G. *Appl. Phys. Lett.* **1964**, *4*, 182–184.

5. Pickett, W. E. *Rev. Mod. Phys.* **1989**, *61*, 433–512.

6. Jin, S.; Tiefel, T. H.; McCormack, M.; Fastnacht, R. A.; Ramesh, R.; Chen, L. H. *Science* **1994**, *264*, 413–415.

7. Skintuna, B.; Lamari–Darkrim, F.; Hirscher, M. *Int. J. Hydrogen Energ.* **2007**, *32*,1121–1140.

8. Li, B.; Wang, L.; Kang, B.; Wang, P.; Qui, Y. *Sol. Energ. Mat. Sol. C.* **2006**, *90*, 549–573.

9. Singhal, S. C. *Solid State Ionics*. **2000**, *135*, 305–313.

*10.* Patil, A.; Patil, V.; Shin, D. W.; Choi, J.–W.; Paik, D.–S.; Yoon, S.–J. *Mater. Res. Bull*. **2008**, *43*, 1913–1942.

11. Wang, X.; Peng, J.; Alimaje, K.; Zhang, Z.; Shi, Z.; *Inorg. Chem. Comm.*, **2013** , *36* , 141–145.

12. Proust, A,; Matt, B.; Villanneau, R.; Guillemot, G.; Gouzerha, P.; Izzeta, G.; *Chem. Soc. Rev*., **2012**, *41*, 7605–7622.

13. Pope, M.; Muller, A.; *Angew. Chem., Int. Ed. Engl.*, **1991**, *30*, 34.

14. Rhule, J.; Hill, C.; Judd, D.; Schinazi, R.; *Chemical Reviews*, **1998**, *98*, 327-357.

15. Miras, H.; Yan, J.; Long, D.; Cronin, L.; *Chem. Soc. Rev.*, **2012,** *41*, 7403-7430.

16. Long, D.; Tsunashima, R.; Cronin, L.; *Angew. Chem. Int. Ed*., **2010**, 49, 1736 – 1758.

17. Nohra, B.; Moll, H.; Albelo, L.; Mialane, P.; Marrot, J.; Mellot-Draznieks, C.; O'Keeffe, M.; Biboum, R.; Lemaire, J.; Keita, B.; Nadjo, L;. Dolbecq, A.; *J. Am. Chem. Soc*. **2011**, *133*, 13363–13374.

18. Du, D.; Qin, J.; Li,D.; Su, Z.; Lan, Y.; *Chem. Soc. Rev.***2014**, DOI: 10.1039/c3cs60404g

19. Wang,Y.; Ye,L.; Wang, T.; Cui, X.; Shi, S.; Wanga, S.; Xu, J.; *Dalton Trans*., **2010**, *39*, 1916–1919.

20. Calzado, C.; Clemente-Juan, J.; Coronado, E.; Gaita-Arino, A.; Suaud, N.; *Inorg. Chem*. **2008**, *47*, 5889-5901.

21. Queen, W.; PhD Dissertation, Clemson University, Clemson, SC, **2009**.

22. West, J.; PhD Dissertation, Clemson University, Clemson, SC, **2012**.

23. Hester, B and Sulejmanovic, D. unpublished research, Clemson University, **2012**.

24. Keggin. J.; *Proc. Roy. Soc*., **1934**, *A 144*, 75-100.

# CHAPTER TWO

# SYNTHESIS AND CHARACTERIZATION OF $(H_2bpy)(Hbpy)_2(V_{15}O_{36}Cl)\cdot n(H_2O)$ FEATURING NON-COVALENT INTERACTIONS

## Introduction

Rational design of inorganic-organic extended hybrids has seen increased research activities due to their potential applications in catalysis, nonlinear optics, energy storage, and etc[1]. The goal of this study is to seek optimal conditions under which the water-soluble polyoxometalate (POM) anions interact with aromatic organic ligands to form self-assembled frameworks. As known, there are many factors which govern the synthesis of extended inorganic-organic hybrids, e.g., temperature, pressure, heating/cooling rate, pH of the solution and the mixture of solvents. The resulting solids provide new hybrids made of POM anions and aromatic organic lattices for the fundamental study of bonding at the donor–acceptor interface. To entice the formation of donor-acceptor relationship through anion-π interaction,[20] we have first selected organic molecules that contain hetero-aromatic rings, 4,4'-bipyridine (bpy, for the simplicity hereafter) in this case, for this conceptual study. The previously synthesized $Cs_5V_{14}As_8O_{42}Cl$ has been used as the source of the selected POM anion for this study.

$Cs_5V_{14}As_8O_{42}Cl$ is a water-soluble salt containing anionic cluster $V_{14}As_8O_{42}Cl^{5-}$, and it is the most reduced vanadium cluster where all V atoms are tetravalent, $V^{4+}$.[2] If the formation of the above mentioned extended solids were to be understood in terms of non-covalent interactions, it would open up a new area of study in synthesis by design of, for instance, porous frameworks of catalytic importance. These frameworks would be

multifunctional with respect to redox chemistry (due to the multiple redox centers in POM clusters) and chemical selectivity (due to organic functional groups). In the following sections, the synthesis and structural characterization of the initial investigation based on a newly discovered hybrid solid, $(H_2bpy)(Hbpy)_2(V_{15}O_{36}Cl)\cdot n(H_2O)$, are discussed.

## Synthesis of bpy-$V_{15}$

The polyoxovanadate $Cs_5V_{14}As_8O_{42}Cl$ was synthesized according to the procedures reported in ref. 2 *via* the high-temperature, solid-state reaction of a stoichiometric mixture (0.75 g) of CsCl, $CsVO_3$, VO, $VO_2$, and $As_2O_3$ in 1:4:2:8:4 mol ratios. The reactants were ground in a nitrogen purged dry box and then placed in a quartz ampoule. The ampoule was sealed under vacuum and then heated to 650 $^oC$ at a rate of $1^oC$ /min followed by isothermal heating for three days. The reaction was then furnace-cooled to room temperature and the product was retrieved as brown polycrystalline powder. The phase was confirmed according to the matched powder X-ray diffraction (PXRD) patterns shown in Figure 2.1.

The original crystal growth of $(H_2bpy)(Hbpy)_2(V_{15}O_{36}Cl)\cdot n(H_2O)$, **bpy-$V_{15}$** hereafter, was observed in a reaction to explore $V_{14}As_8O_{42}Cl^{5-}$-containing, inorganic-organic hybrid phases. In an original reaction, a total of 0.125 g of $Cs_5V_{14}As_8O_{42}Cl$, $Mn(OAc)_2$ (OAc = acetate), and 4,4'-bipyridine (bpy) were loaded in a 1:1:10 molar ratio, respectively to synthesize extended POV-Mn-bpy frameworks.[22] Deionized water (5 mL) and ethanol (5 mL)were added to the mixture and the pH was adjusted to 3.5 by

dropwise addition of 2M HCl. The reactants were stirred briefly for 1 min before being transferred to a 20 mL Teflon-lined hydrothermal container. The stainless steel hydrothermal bomb was then heated to 160 $^{o}$C over a period of one hour and was isothermed for 15 hours under autogenous pressure. The reaction was then slowly cooled to 25 $^{o}$C over a period of 60 hours. Solid product was filtered and washed using deionized (DI) water via suction filtration method. Dark green (almost black) column-like (~20 % estimated yield) crystals, as shown in Fig. 2.3, left, were isolated under an optical microscope and were mounted for single crystal X-ray diffraction (SXRD) study. The product also contained an unidentified green polycrystalline phase as shown in Figure 2.2 (~80 % estimated yield). An effort was made to identify the unknown green powder by comparing its pattern with one of the unpublished compounds, $(H_2bpy)_2{\cdot}V_{14}As_8O_{42}Cl$, synthesized under similar reaction conditions prior to this study,[25] but it was unsuccessful as illustrated by Figure 2.2.

## Structure Determination

The single crystal X-ray diffraction data were collected at room temperature on a four-circle Rigaku AFC8 diffractometer equipped with a Mercury CCD area detector, Mo Kα (λ= 0.71073 Å) radiation. An empirical multiscan absorption correction was applied using *REQAB*, a subroutine of the *CrystalClear* software package. Refinement of the crystal structures using a full-matrix, least-squares technique was performed using the SHELXTL package software (version 6.1).[3-6]

Hydrogen atoms that form C−H covalent bonds were added using calculated positions. Hydrogens attached to the nitrogen atoms were able to be intuitively selected from the difference map. Table 2.5 shows selected angles of bpy molecule where the sum of ∠C=N–C , ∠C=N–H and ∠H–N–C = ~360, which suggests that the hydrogen atoms are in the same plane as the aromatic rings as anticipated.[16] Disordered water molecules were added by finding the oxygen atoms from the difference map. The occupancy of these oxygen atoms was refined using the SHELXTL software package yielding partial occupancy.

Attempts in further refinement to include hydrogen atoms of water molecules from the difference map were made but unsuccessful possibly because of the partial occupancy of oxygen and the inherent difficulty of finding hydrogen atoms using SXRD. The crystallographic information file (CIF) was subject to the evaluation by CheckCif, an online service provided by the International Union of Crystallography (IUCr). The CheckCif resulted in zero level-A alerts but one level-B alert corresponding to O37 atom of water molecule. This alert is due to the absence of associated hydrogen atoms.

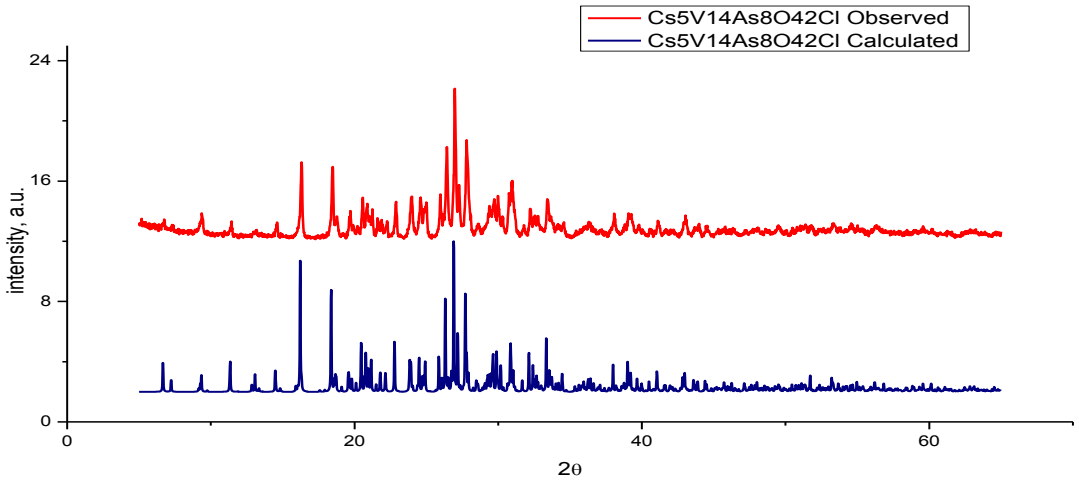


Figure 2.1**:** PXRD patterns of $Cs_5V_{14}As_8O_{42}Cl$ showing a good agreement between (top) the observed and (bottom) theoretical plots. The latter is calculated using the crystallographic data acquired from SXRD studies.

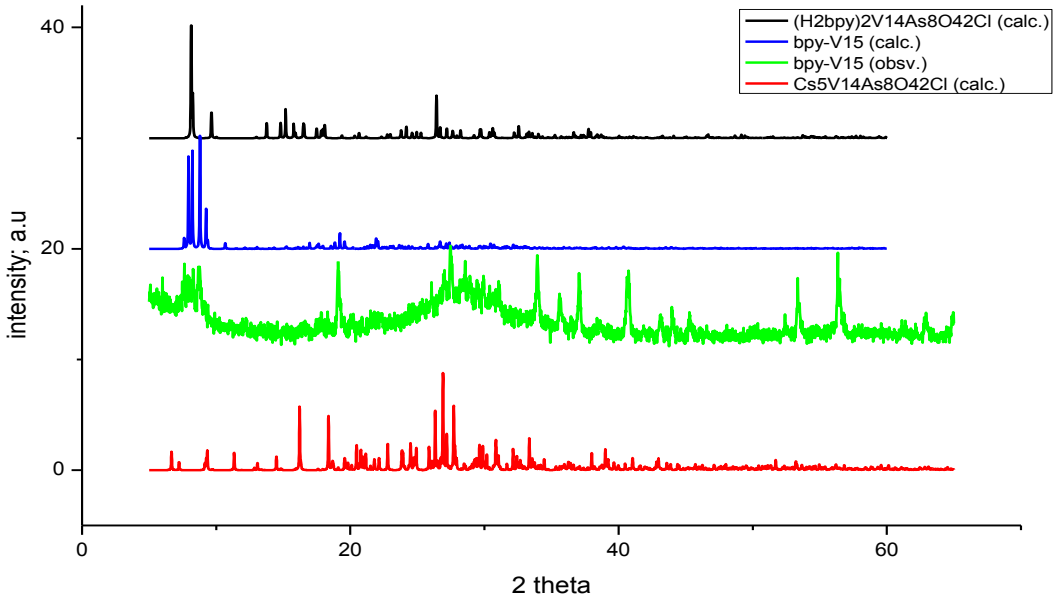


Figure 2.2: (bottom to top) Calculated PXRD patterns of $Cs_5V_{14}As_8O_{42}Cl$ (red), observed PXRD of bpy-$V_{15}$ showing extra reflections (green), calculated bpy-V15 (blue), and calculated $(H_2bpy)_2{\cdot}V_{14}As_8O_{42}Cl$ unpublished work from our group.

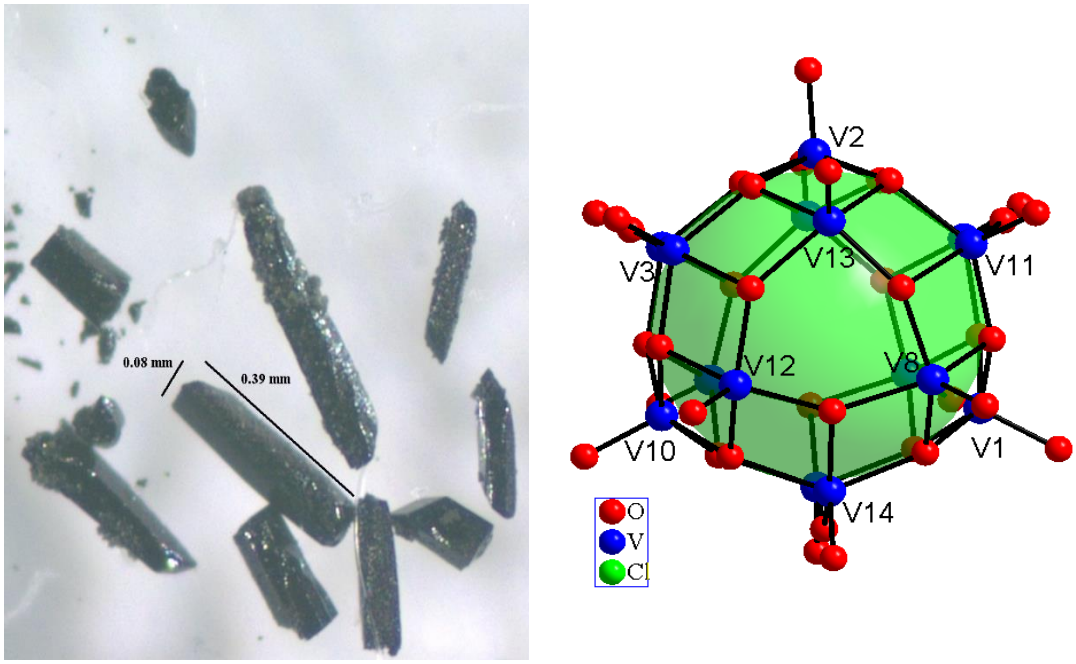


Figure 2.3: (left) Optical image of selected crystals showing column-like crystals (in dark green color) of $(H_2bpy)(Hbpy)_2(V_{15}O_{36}Cl)\cdot n(H_2O)$. (right) The $(V_{15}O_{36}Cl)^{4-}$ cluster viewed along the pseudo three-fold axis.

## Results and Discussion

As mentioned above, **bpy-$V_{15}$** was synthesized using the water soluble $Cs_5V_{14}As_8O_{42}Cl$ polyoxometalate compound as a precursor under hydrothermal reaction conditions. From initial observation of the structure and the empirical formula, it can be seen that the starting polyoxovanadate - $\{V_{14}As_8O_{42}Cl\}^{5-}$ cluster was not incorporated, but $\{V_{15}O_{36}Cl\}^{4-}$. The potential reason for this is that the conditions under which the reaction took place may have led to the decomposition of $Cs_5V_{14}As_8O_{42}Cl$. It is suspected that the temperature as well as the acidity of the reaction played a key role in the defragmentation of the $V_{14}As_8O_{42}Cl^{5-}$ cluster and formed simple oxides *in situ*. Subsequently, the fragmented vanadium-oxides under acidic conditions readily combined to form the title polyoxometalate cluster compound. This in general is anticipated as the formation of POMs in the presence of simple early transition metal oxides under acidic conditions is well-documented in the POM literature.[7]

Dark green, column-like crystals of **bpy-$V_{15}$** crystallize in the monoclinic crystal system, space group $P\ 2_1/c$ (No. 14) with the unit cell dimensions of $a$ = 16.563(3) Å, $b$ = 12.655(3) Å, $c$ = 29.142(6) Å, $\beta$ = 92.06(3) $^{o}$, $V$ = 6104.35(200) Å$^3$. Table 2.1 shows crystallographic data for the titled compound. According to the structural formula obtained from the single-crystal X-ray diffraction studies and the bond valence sums calculations, title compound is mixed valent with formally nine $V^{5+}$ and six $V^{4+}$ ions. The charges of the vanadium cations are delocalized as suggested by the results of the bond valence sum calculations in Table 2.2. The calculated bond valence sum for some V atoms show a value between 4 and 5 (for example V8 has an averaged value of 4.5)

suggesting a possible delocalization for the charge in cluster environment. Nevertheless, adding up the values of bond valence sum of all vanadium atoms gives a total value of (positive charge of) 68.7 which is close to the expected formal charge of 69+ based on $9 \times V^{5+}$ and $6 \times V^{4+}$. The structure of the $\{V_{15}O_{36}Cl\}^{4-}$ anion- Figure 2.2 right- is similar to the previously reported $\{V_{15}O_{36}Cl\}^{4-}$ clusters.[8,23] The anion in the title compound is composed of 15 crystallographically independent vanadium atoms which adopt the square pyramidal geometry with respect to the oxygen atoms. The short apical or the vanadyl V=O bonds are pointing away from the center of the cluster with bond distances ranging from 1.584(4) Å for V11 to 1.612(4) Å for V7. These 15 vanadium atoms are connected through 18 $\mu_3$- and three $\mu_2$-oxo bridges forming a 36-member cage encapsulating a chlorine atom. The bond distances of vanadium atoms to $\mu_3$- and $\mu_2$-oxygen atoms range from 1.732(4) Å to 2.151(4) Å and are close to the expected 1.90-1.94 Å, the sum of the crystal radii for $V^{4+}$, $V^{5+}$ (0.72 Å and 0.68 Å) and $O^{2-}$(1.22 Å).[9] Notably, the average of all non-vandyl bonds are 1.9205 Å and is in the range of expected sum of the crystal radii for V and O. The shortest V-V distance is 2.8109(12) Å between V11 and V13 atoms as shown in Figure 2.7 top.

$\{V_{15}O_{36}Cl\}^{4-}$ anion is surrounded by three crystallographically unique 4,4'-bipyridine (bpy) units. One of the bpy molecules is fully protonated with hydrogen atoms, H4A and H6A which are attached to the nitrogen atoms, N4 and N6, with N-H distance of 0.805(8) Å and 0.862(8) Å, respectively.[16,17] H4A and H6A participate in hydrogen bonding with the neighbouring oxygen atoms (O35 and O21, respectively) of the $\{V_{15}O_{36}Cl\}^{4-}$ anion to form an infinite chain of $[H_2bpy\text{-}\{V_{15}O_{36}Cl\}]_\infty^{2-}$ as shown in

Figures 2.4 and 2.5. The hydrogen bond distance between H4A and O35 is 1.810(85) Å and between H6A and O21 is 1.794(80) Å. The strength of this hydrogen bonding is moderate as the total bond length of N−H···O 2.6 Å which is within the anticipated range of moderate hydrogen bonding 2.5-3.2 Å.[16] The remaining two bpy molecules are protonated only at one of the nitrogen atoms (N1 and N5, respectively). N1 is bonded to H1A with the distance of 0.712(86) Å while the distance between N5 and H5A is 0.955(87) Å. H1A participates in hydrogen bonding with a water molecule (O38) with the distance of 1.997(88) Å. H5A is hydrogen bonded to O36 on the $\{V_{15}O_{36}Cl\}^{4-}$ anion with the distance of 1.828(87) Å. Table 2.3 and Table 2.4 show some selected bond distances and angles between the atoms.

In addition to hydrogen bonding, π-π stacking exists between the bpy rings containing N6 and N2; and those containing N4 and N5, as shown in Figure 2.6. The distances between the two rings range from 3.5 to 3.8 Å similar to the distances 3.5~3.9 Å in reported compounds.[10,12,19] Another donor–acceptor interaction is observed in the structure where oxygen atom of the cluster interacts with bpy ring. This type of anion-π interaction is favourable and observed in some coordination compounds where the major interaction is made of direct coordination between POM anions and metal cations instead. Nevertheless, the latter also exhibits electron-rich anionic clusters donating charges to electron-poor, hetero-aromatic rings like bpy.[20-21] In the title compound, the anion-π interaction stabilizes the two layers as shown in Figure 7.[12-15] O15 which is covalently bonded only to V10 interacts with bpy ring (N3) in the distance of 3.71A. O16 $\mu_2$-oxygen shared by V10 and V15 is pointing at the center of the (N5) bpy ring with the distance of

3.88 Å suggesting another anion-π interaction. In Summary, $\{V_{15}O_{36}Cl\}^{4-}$ anion has 5 oxygen atoms showing non-covalent interactions with bpy. O35 and O21 form hydrogen bonding from opposite sides of the cluster along the extended chain, and O36 is also forming hydrogen bonding but to singly protonated bpy (N5). O15 and O16 participate in anion–π interactions to bpy (N3) and (N5), respectively. With these interactions one would assume a potentially high thermal stability of the product as shown in the TGA study (see the TGA study below).

Infrared spectroscopy measurements were performed using a Thermo Scientific Nicolet IR200 instrument. KBr powder was dried at 140 $^{o}$C in a vacuum oven for two hours and was placed inside a desiccator before being used to make transparent pellets. Approximately 0.5 mg of **bpy-V15** single crystals were selected and mixed in with KBr to make the sample pellet. Infrared spectroscopy was used to confirm the presence of water as well as the presence of hydrogen in N-H, at around 1605cm$^{-1}$, as shown in Figure 8.[18,24] It also shows the distinctive peaks for V = O stretching and V-O-V bending around 986 and 651 cm$^{-1}$, respectively. The presence of water is confirmed by the broad peak at 3422 cm$^{-1}$. Aromatic C = C and C = N peaks are observed between 1400-1630 cm$^{-1}$, namely the 1625 cm$^{-1}$ and 1484 cm$^{-1}$ , respectively.

Thermogravimetric analysis used to determine a material's thermal stability and provides a quantitative measurement of mass change in materials typically associated with the decomposition of volatile species. It can be observed that the title compound decomposes in two distinct stages between room temperature and 600 $^{o}$C. The decomposition at lower temperatures (< 200 $^{o}$C) is likely the result of losing water

molecules. At the onset around 100 $^{o}$C the weight loss percent is about 6 % which corresponds to water evaporation. This observation is in close approximate to the calculated water molecules weight loss 5.3% (n = 5.7) as shown in Figure 8. The calculated water molecules are obtained by adding up the oxygen partial occupancy (see Table 2.6) which gave 5.7 water molecules.

Another major weight loss observed at the onset of 435 $^{o}$C is due to the loss of bpy during the heating course. Notably, the calculated weight loss from 435 ~ 465 $^{o}$C is 14 % which is comparable with the theoretical weight loss of 16.1% for 2 bpy.

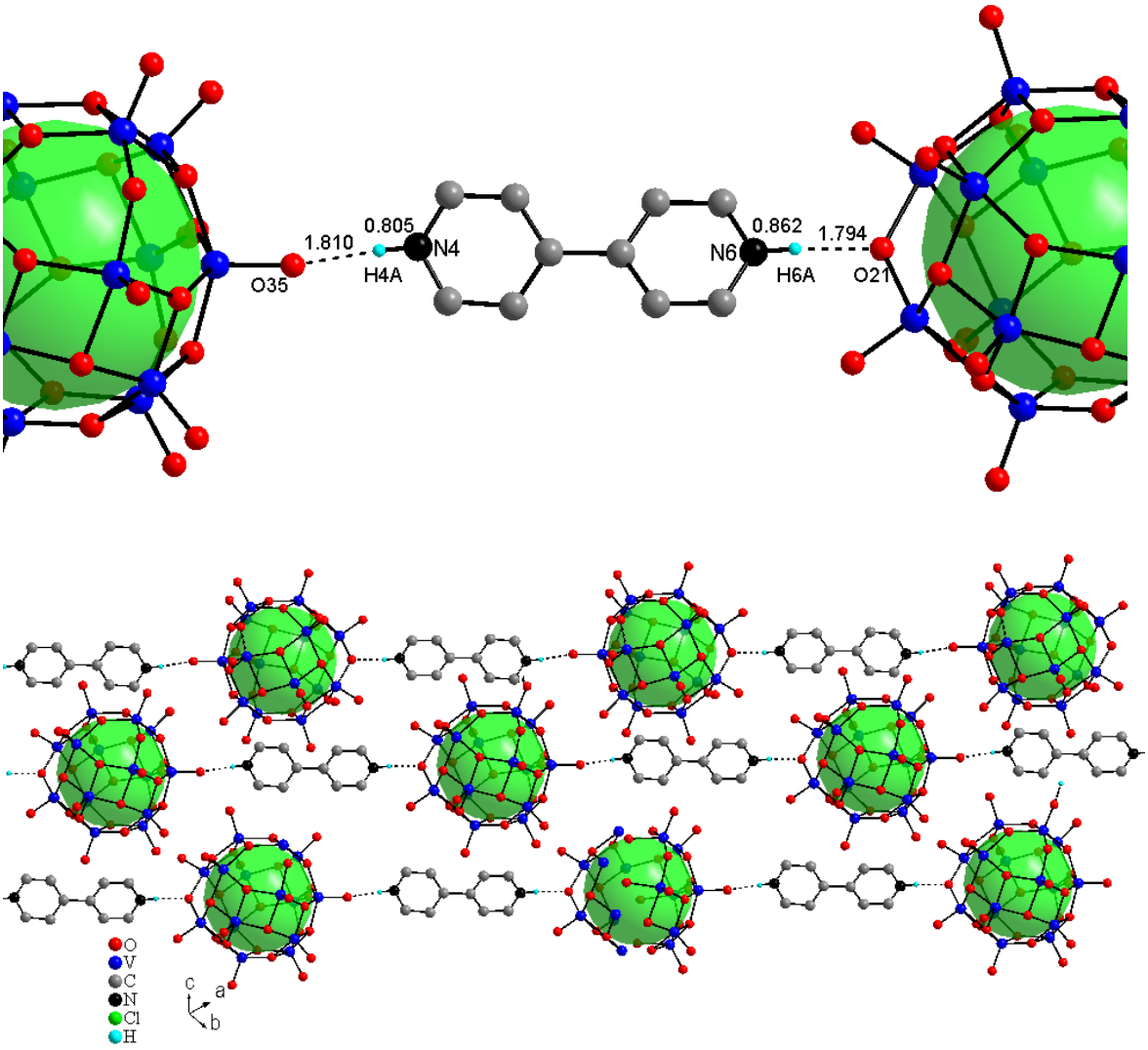


Figure 2.4: Partial structure showing the chain of alternating $H_2$bpy-$V_{15}$ along [110]. The unique bpy molecule in top inset that is fully protonated, $H_2$bpy, is forming the linker through H···O hydrogen bonds to extend the chain. The hydrogen bonding is formed between the N-H bond and oxygen atom of the cluster.

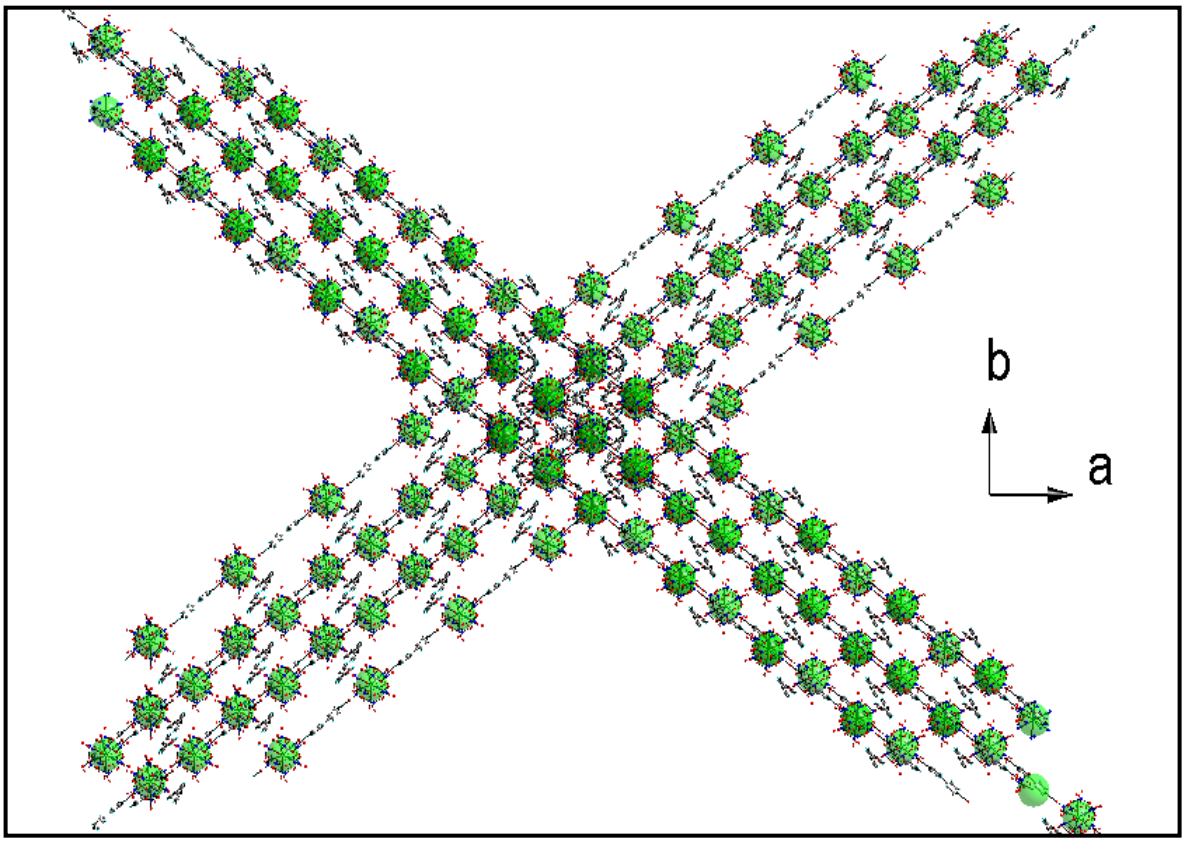


Figure 2.5: Projected view showing the orthogonally arranged infinite chains of bpy-$V_{15}$ along the ab diagonals.

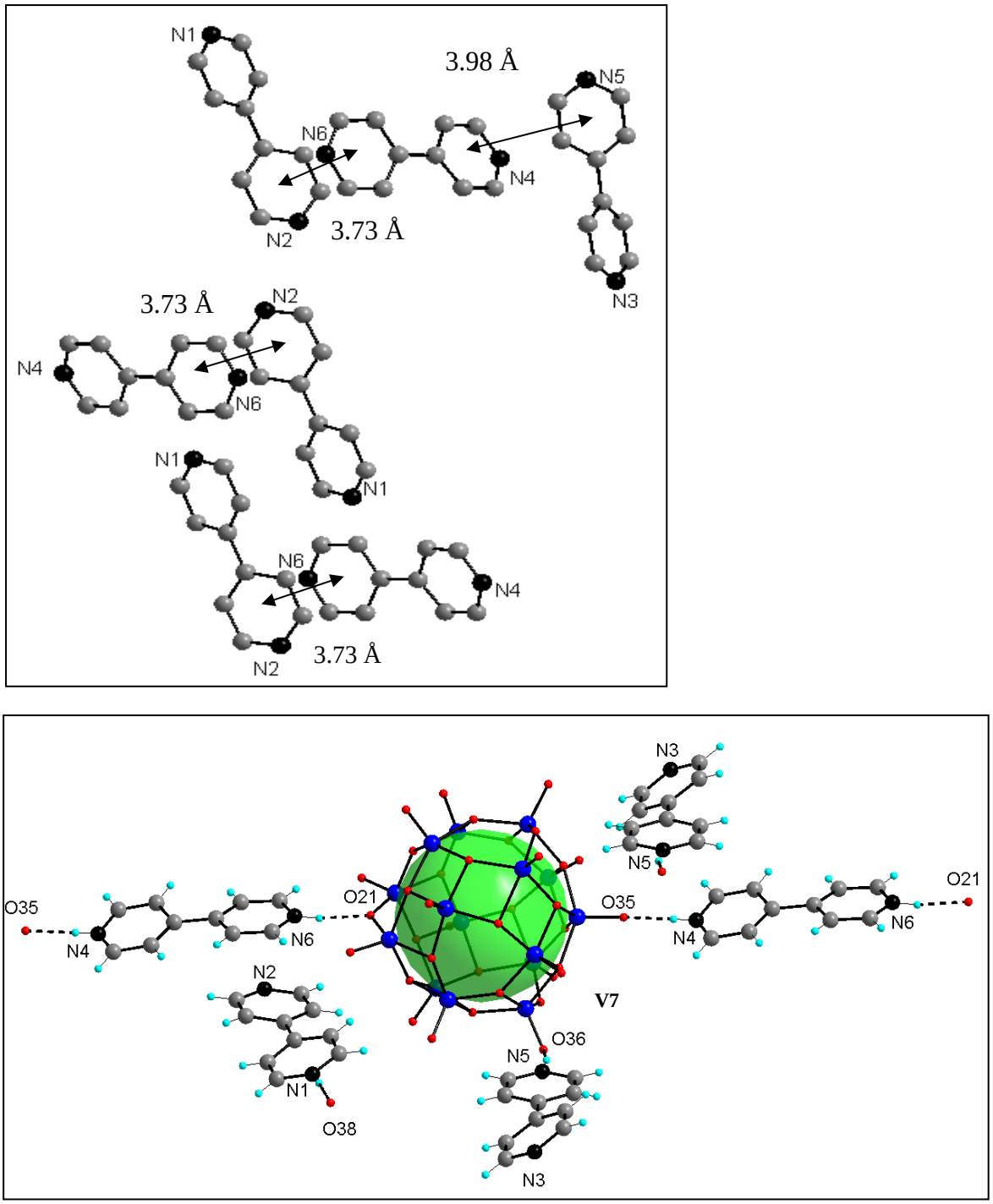


Figure 2.6: (top) π-π stacking between bpy rings where the ring in top of each other and distance ranges from 3.73 to 3.98 Å. (bottom) three crystallographically unique bpy.

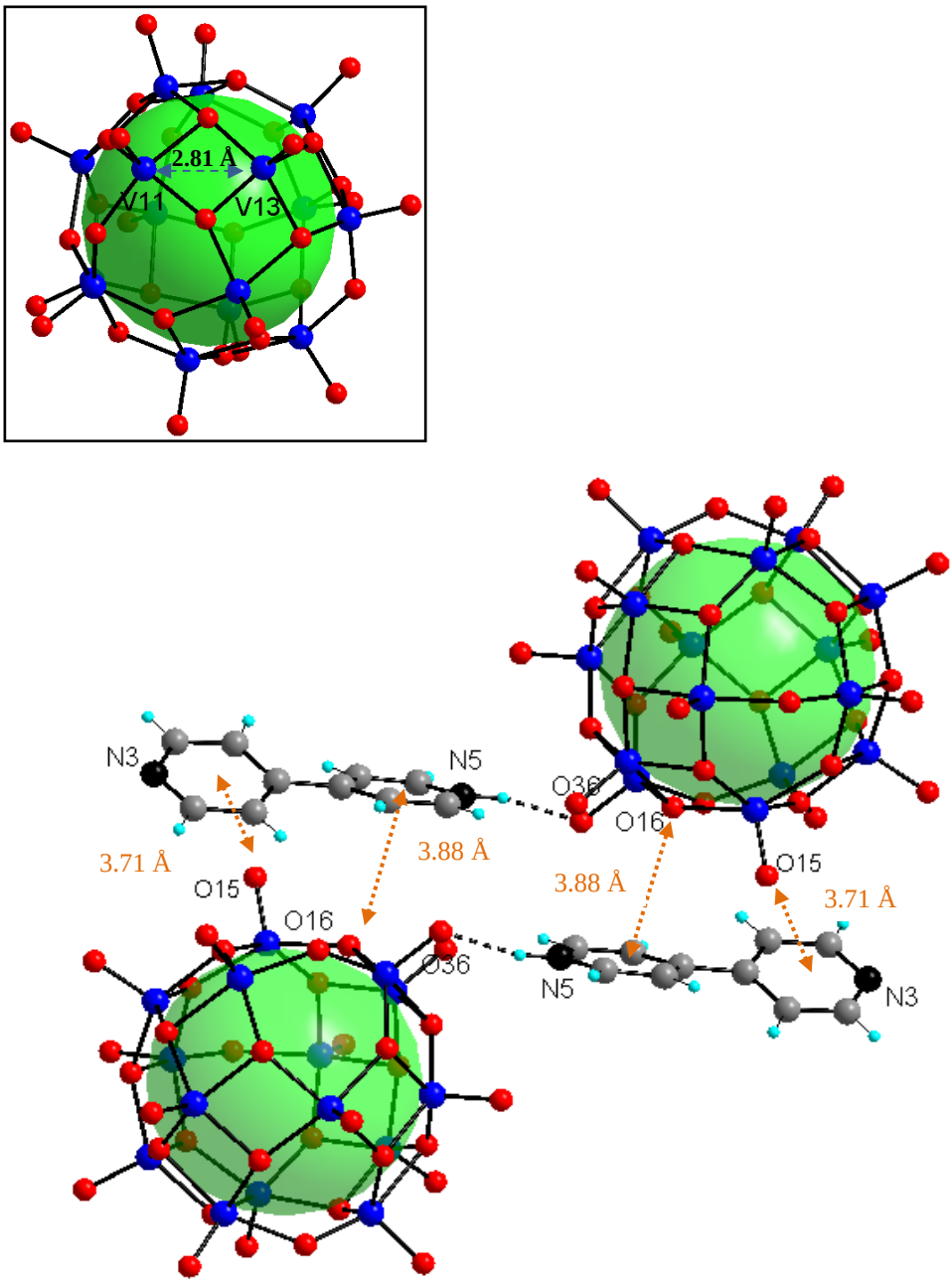


Figure 2.7: (Top inset) The shortest V-V bond 2.81 Å between V11 and V13 and (bottom) their relative positions with two nearest bpys showing donor –acceptor interactions through O15 with the distance to the center of the ring (N3) of 3.71 Å, and through O16 with distance to the center of the other ring (N5) of 3.88 Å.

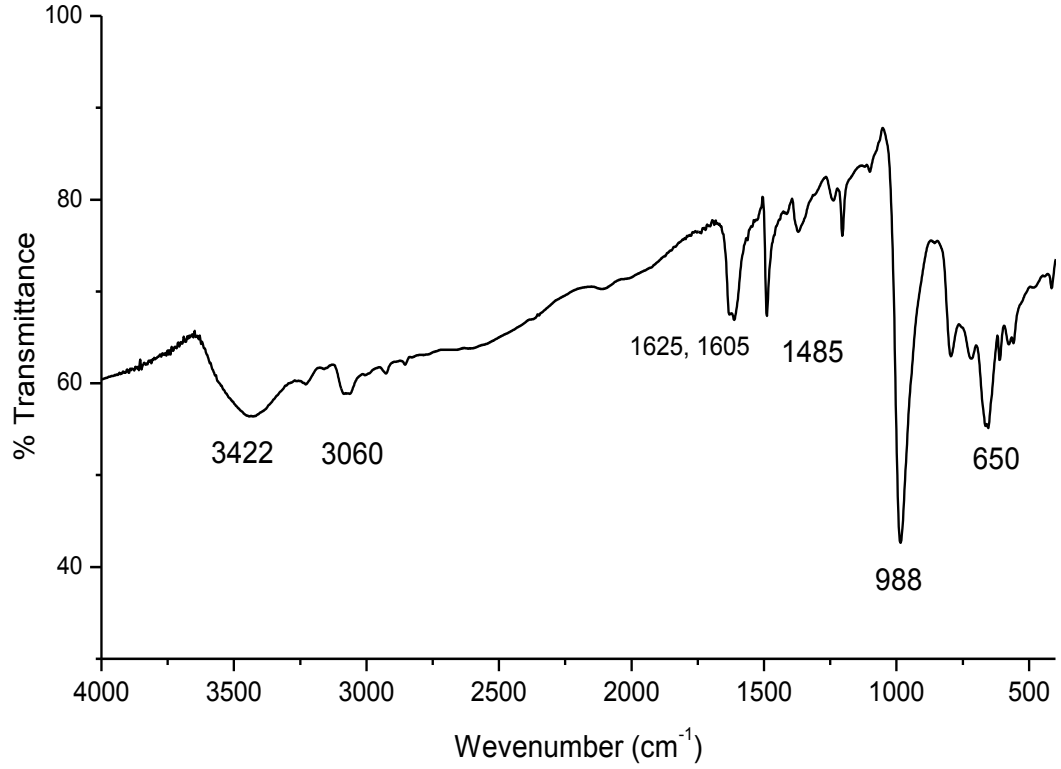


Figure 2.8: IR spectra showing peaks at 650 and 988 cm–1 corresponding to υV-O and υV=O stretching of the $V_{15}O_{36}$ cluster, and broad peak at 3422 $cm^{-1}$ of water molecules in the structure. Peaks at 1485, 1605 and 1625 $cm^{-1}$ are corresponding to C = C, N-H and C = N, respectively.

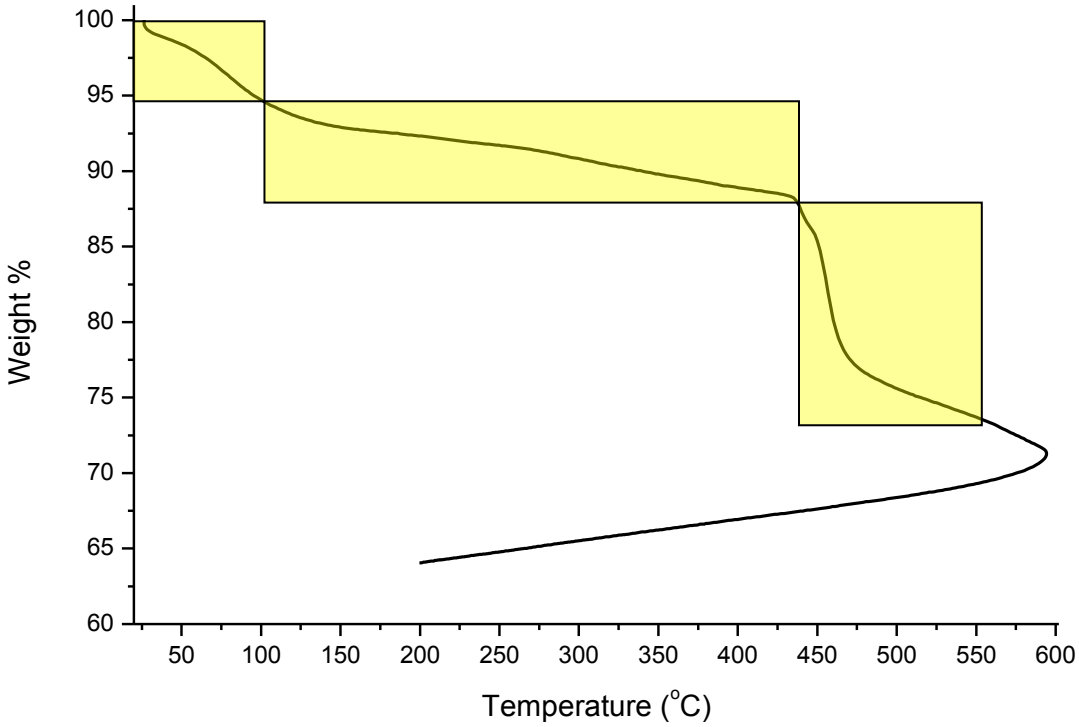


Figure 2.9: Thermogravimetric analysis of bpy-V15 in nitrogen showing the decomposition offset at ca. 100 $^{o}$C and onset at ca. 435 $^{o}$C. The observed weight loss corresponding to the former is ca. 6%. The second weight loss is corresponding to two bpy molecules 16 %.

Table 2.1: Crystallographic data for $(H_2bpy)(Hbpy)_2(V_{15}O_{36}Cl)\cdot n(H_2O)$

| | |
|---|---|
| Empirical formula | $V_{15}O_{41.71}C_{30}N_6H_{28}$ |
| Formula weight (amu) | 1939.49 |
| Color/shape | Dark green column |
| Crystal system | Monoclinic |
| Space group, Z | $P2_1/c$ (14), 4 |
| T, °K | 200 |
| a (Å) | 16.563(3) |
| b (Å) | 12.655(3) |
| c (Å) | 29.142(6) |
| ß ° | 92.06(3) |
| Cell volume Å3 | 6104(2) |
| Density, calcd ( g/cm3) | 4.823 |
| μ (Mo Kα), $mm^{-1}$ | 2.33 |
| $F_{000}$ | 3824 |
| Data/restraints/parameters | 10678/0/874 |
| Final R1 / wR2[I > 2σ(I)] | 0.0498/0.1291 |
| R1/wR2 (all data) | 0.0611/0.143 |
| GOF | 1.114 |

Table 2.2: Bond valence sums calculations showing the V-O distances in Å. The bolded numbers are assigned oxidation states

| **V1 -O distances** | 4+ | 5+ | **V2 - O distances** | 4+ | 5+ | **V3 - O distances** | 4+ | 5+ |
|---|---|---|---|---|---|---|---|---|
| 1.610 | 1.600 | 1.685 | 1.601 | 1.640 | 1.726 | 1.600 | 1.644 | 1.731 |
| 1.947 | 0.644 | 0.678 | 1.957 | 0.627 | 0.660 | 1.773 | 1.030 | 1.084 |
| 1.950 | 0.638 | 0.672 | 1.973 | 0.600 | 0.632 | 1.879 | 0.774 | 0.814 |
| 1.957 | 0.627 | 0.660 | 1.974 | 0.598 | 0.630 | 1.880 | 0.771 | 0.812 |
| 1.958 | 0.625 | 0.658 | 1.976 | 0.595 | 0.627 | 2.046 | 0.493 | 0.519 |
| **4** | 4.134 | 4.352 | **4** | 4.060 | 4.274 | **5** | 4.712 | 4.960 |
| **V4 - O distances** | 4+ | 5+ | **V5 - O distances** | 4+ | 5+ | **V6 - O distances** | 4+ | 5+ |
| 1.596 | 1.662 | 1.750 | 1.601 | 1.640 | 1.726 | 1.590 | 1.689 | 1.778 |
| 1.907 | 0.717 | 0.755 | 1.732 | 1.151 | 1.212 | 1.854 | 0.828 | 0.871 |
| 1.907 | 0.717 | 0.755 | 1.886 | 0.759 | 0.799 | 1.864 | 0.806 | 0.848 |
| 1.913 | 0.706 | 0.743 | 1.887 | 0.757 | 0.797 | 1.919 | 0.694 | 0.731 |
| 2.011 | 0.541 | 0.570 | 2.151 | 0.371 | 0.390 | 1.926 | 0.681 | 0.717 |
| **4** | 4.344 | 4.572 | **5** | 4.678 | 4.924 | **5** | 4.698 | 4.946 |
| **V7 -O distances** | 4+ | 5+ | **V8 - O distances** | 4+ | 5+ | **V9 - O distances** | 4+ | 5+ |
| 1.612 | 1.592 | 1.676 | 1.611 | 1.596 | 1.680 | 1.605 | 1.622 | 1.708 |
| 1.829 | 0.885 | 0.932 | 1.891 | 0.749 | 0.788 | 1.881 | 0.769 | 0.810 |
| 1.905 | 0.721 | 0.759 | 1.902 | 0.727 | 0.765 | 1.894 | 0.743 | 0.782 |
| 1.906 | 0.719 | 0.757 | 1.934 | 0.667 | 0.702 | 1.894 | 0.743 | 0.782 |
| 2.040 | 0.501 | 0.527 | 1.934 | 0.667 | 0.702 | 1.912 | 0.708 | 0.745 |
| **5** | 4.418 | 4.651 | **4** | 4.405 | 4.637 | **5** | 4.585 | 4.826 |
| **V10 -O distances** | 4+ | 5+ | **V11 - O distances** | 4+ | 5+ | **V12 - O distances** | 4+ | 5+ |
| 1.597 | 1.658 | 1.745 | 1.591 | 1.685 | 1.774 | 1.595 | 1.667 | 1.754 |
| 1.965 | 0.613 | 0.645 | 1.910 | 0.711 | 0.749 | 1.811 | 0.930 | 0.979 |
| 1.975 | 0.597 | 0.628 | 1.912 | 0.708 | 0.745 | 1.892 | 0.747 | 0.786 |
| 1.977 | 0.594 | 0.625 | 1.915 | 0.702 | 0.739 | 1.908 | 0.715 | 0.753 |
| 1.985 | 0.581 | 0.611 | 2.017 | 0.533 | 0.561 | 1.932 | 0.670 | 0.706 |
| **4** | 4.042 | 4.255 | **4** | 4.338 | 4.567 | **5** | 4.729 | 4.978 |
| **V13 -O distances** | 4+ | 5+ | **V14 - O distances** | 4+ | 5+ | **V15 - O distances** | 4+ | 5+ |
| 1.603 | 1.631 | 1.717 | 1.601 | 1.640 | 1.726 | 1.610 | 1.600 | 1.685 |
| 1.826 | 0.893 | 0.940 | 1.803 | 0.950 | 1.000 | 1.894 | 0.743 | 0.782 |
| 1.885 | 0.761 | 0.801 | 1.888 | 0.755 | 0.795 | 1.894 | 0.743 | 0.782 |
| 1.938 | 0.660 | 0.694 | 1.900 | 0.731 | 0.769 | 1.910 | 0.711 | 0.749 |
| 1.938 | 0.660 | 0.694 | 2.089 | 0.439 | 0.462 | 1.917 | 0.698 | 0.735 |
| **5** | 4.604 | 4.846 | **5** | 4.514 | 4.752 | **5** | 4.496 | 4.732 |

Table 2.3**:** Selected bond distances for of bpy-$V_{15}$

| Bond | distances (A) | Bond | distances (A) |
|---|---|---|---|
| V1—O35 | 1.610 (3) | V6—O30 | 1.596 (4) |
| V1—O6 | 1.948 (4) | V6—O19 | 1.853 (4) |
| V1—O3 | 1.949 (3) | V6—O24 | 1.861 (3) |
| V1—O5 | 1.958 (4) | V6—O5 | 1.920 (4) |
| V1—O2 | 1.958 (4) | V6—O2 | 1.925 (3) |
| V1—V8 | 2.9644 (15) | V6—V7 | 2.9149 (14) |
| V1—V6 | 3.0043 (14) | V7—O36 | 1.612 (4) |
| V2—O31 | 1.599 (3) | V7—O20 | 1.832 (4) |
| V2—O9 | 1.957 (3) | V7—O16 | 1.902 (3) |
| V2—O8 | 1.971 (4) | V7—O5 | 1.906 (3) |
| V2—O14 | 1.973 (3) | V7—O24 | 2.039 (4) |
| V2—O11 | 1.977 (3) | V7—V15 | 2.9428 (14) |
| V2—V9 | 2.9752 (15) | V8—O32 | 1.608 (4) |
| V2—V13 | 2.9962 (14) | V8—O17 | 1.890 (3) |
| V3—O18 | 1.600 (3) | V8—O3 | 1.900 (4) |
| V3—O21 | 1.771 (3) | V8—O6 | 1.933 (4) |
| V3—O14 | 1.880 (3) | V8—O29 | 1.935 (3) |
| V3—O1 | 1.882 (3) | V8—V11 | 2.8452 (14) |
| V3—O7 | 2.049 (3) | V8—V14 | 3.0127 (13) |
| V3—V12 | 2.9865 (14) | V9—O33 | 1.600 (4) |
| V3—V13 | 3.0147 (12) | V9—O10 | 1.884 (3) |
| V4—O13 | 1.598 (3) | V9—O9 | 1.893 (3) |
| V4—O9 | 1.906 (3) | V9—O19 | 1.895 (3) |
| V4—O4 | 1.908 (4) | V9—O8 | 1.915 (4) |
| V4—O21 | 1.910 (3) | V10—O15 | 1.593 (3) |
| V4—O10 | 2.011 (3) | V10—O4 | 1.967 (4) |
| V4—V9 | 2.8791 (13) | V10—O16 | 1.976 (4) |
| V4—V15 | 2.8957 (13) | V10—O12 | 1.980 (4) |
| V5—O22 | 1.604 (4) | V10—O1 | 1.982 (4) |
| V5—O23 | 1.732 (4) | V10—V15 | 2.9911 (14) |
| V5—O2 | 1.887 (3) | V10—V12 | 3.0220 (14) |
| V5—O8 | 1.888 (3) | V11—O25 | 1.584 (4) |
| V5—O19 | 2.151 (4) | V11—O3 | 1.908 (3) |
| V5—V6 | 3.0099 (13) | V11—O23 | 1.912 (4) |
| V5—V9 | 3.0131 (13) | V11—O11 | 1.915 (3) |

Table 2.3 (Continued.): Selected bond distances for of bpy-$V_{15}$

| Bond | distances (A) | Bond | distances (A) |
|---|---|---|---|
| V11—O17 | 2.017 (4) | N5—C24 | 1.325 (10) |
| V11—V13 | 2.8109 (12) | N5—C37 | 1.343 (10) |
| V12—O34 | 1.599 (4) | N6—C10 | 1.325 (7) |
| V12—O29 | 1.812 (3) | N6—C26 | 1.345 (8) |
| V12—O7 | 1.891 (3) | C1—C20 | 1.409 (11) |
| V12—O12 | 1.902 (4) | C6—C9 | 1.359 (8) |
| V12—O1 | 1.931 (3) | C7—C37 | 1.364 (11) |
| V12—V14 | 2.9171 (14) | C7—C4 | 1.391 (9) |
| V13—O28 | 1.600 (4) | C8—C38 | 1.364 (9) |
| V13—O17 | 1.829 (3) | C9—C5 | 1.378 (7) |
| V13—O11 | 1.885 (4) | C10—C17 | 1.375 (7) |
| V13—O7 | 1.940 (3) | C12—C24 | 1.345 (10) |
| V13—O14 | 1.941 (3) | C12—C4 | 1.393 (8) |
| V14—O26 | 1.600 (4) | C13—C16 | 1.361 (9) |
| V14—O20 | 1.803 (4) | C13—C3 | 1.395 (8) |
| V14—O6 | 1.889 (3) | C17—C2 | 1.390 (7) |
| V14—O12 | 1.900 (3) | C18—C19 | 1.357 (8) |
| V14—O29 | 2.086 (4) | C18—C11 | 1.386 (8) |
| V15—O27 | 1.608 (4) | C20—C14 | 1.388 (9) |
| V15—O10 | 1.892 (4) | C21—C30 | 1.366 (10) |
| V15—O24 | 1.896 (3) | C21—C11 | 1.381 (8) |
| V15—O4 | 1.909 (3) | C22—C26 | 1.363 (8) |
| V15—O16 | 1.920 (4) | C22—C2 | 1.387 (8) |
| N1—C30 | 1.314 (9) | C23—C36 | 1.352 (10) |
| N1—C19 | 1.337 (8) | C23—C3 | 1.400 (8) |
| N2—C1 | 1.312 (11) | C25—C34 | 1.354 (10) |
| N2—C34 | 1.328 (11) | C25—C14 | 1.396 (9) |
| N3—C36 | 1.342 (9) | C38—C5 | 1.359 (8) |
| N3—C16 | 1.344 (9) | C2—C5 | 1.486 (6) |
| N4—C6 | 1.300 (8) | C3—C4 | 1.474 (9) |
| N4—C8 | 1.314 (9) | C11—C14 | 1.479 (8) |

Table 2.4**:** Selected bond angles for bpy-$V_{15}$

| Bond | angle $^{o}$ | Bond | angle $^{o}$ |
|---|---|---|---|
| V4—V15—V10 | 76.34 (4) | V12—O12—V10 | 102.23 (15) |
| V7—V15—V10 | 75.34 (4) | V3—O14—V13 | 104.18 (16) |
| V3—O1—V12 | 103.13 (16) | V3—O14—V2 | 135.92 (18) |
| V3—O1—V10 | 135.7 (2) | V13—O14—V2 | 99.92 (14) |
| V12—O1—V10 | 101.11 (15) | V7—O16—V15 | 100.69 (17) |
| V5—O2—V6 | 104.29 (16) | V7—O16—V10 | 138.4 (2) |
| V5—O2—V1 | 136.45 (19) | V15—O16—V10 | 100.28 (16) |
| V6—O2—V1 | 101.36 (15) | V13—O17—V8 | 146.3 (2) |
| V8—O3—V11 | 96.70 (15) | V13—O17—V11 | 93.81 (16) |
| V8—O3—V1 | 100.75 (15) | V8—O17—V11 | 93.42 (15) |
| V11—O3—V1 | 142.38 (19) | V6—O19—V9 | 140.0 (2) |
| V4—O4—V15 | 98.66 (16) | V6—O19—V5 | 97.20 (16) |
| V4—O4—V10 | 139.78 (19) | V9—O19—V5 | 96.06 (15) |
| V15—O4—V10 | 101.00 (15) | V14—O20—V7 | 130.8 (2) |
| V7—O5—V6 | 99.24 (16) | V3—O21—V4 | 131.03 (17) |
| V7—O5—V1 | 140.2 (2) | V5—O23—V11 | 131.17 (19) |
| V6—O5—V1 | 101.53 (16) | V6—O24—V15 | 140.99 (19) |
| V14—O6—V8 | 104.03 (16) | V6—O24—V7 | 96.62 (15) |
| V14—O6—V1 | 137.6 (2) | V15—O24—V7 | 96.74 (16) |
| V8—O6—V1 | 99.60 (15) | V12—O29—V8 | 141.8 (2) |
| V12—O7—V13 | 136.35 (18) | V12—O29—V14 | 96.67 (16) |
| V12—O7—V3 | 98.48 (15) | V8—O29—V14 | 97.00 (15) |
| V13—O7—V3 | 98.14 (15) | O35—V1—O6 | 105.52 (18) |
| V5—O8—V9 | 104.80 (17) | O35—V1—O3 | 105.39 (17) |
| V5—O8—V2 | 136.5 (2) | O6—V1—O3 | 78.91 (14) |
| V9—O8—V2 | 99.88 (15) | O35—V1—O5 | 107.19 (18) |
| V9—O9—V4 | 98.54 (16) | O6—V1—O5 | 92.84 (15) |
| V9—O9—V2 | 101.19 (14) | O3—V1—O5 | 147.41 (13) |
| V4—O9—V2 | 141.36 (19) | O35—V1—O2 | 107.87 (18) |
| V9—O10—V15 | 143.14 (18) | O6—V1—O2 | 146.61 (13) |
| V9—O10—V4 | 95.26 (15) | O3—V1—O2 | 92.17 (15) |
| V15—O10—V4 | 95.72 (15) | O5—V1—O2 | 77.45 (15) |
| V13—O11—V11 | 95.40 (15) | O35—V1—V8 | 112.62 (16) |
| V13—O11—V2 | 101.71 (15) | O6—V1—V8 | 40.02 (10) |
| V11—O11—V2 | 140.37 (19) | O3—V1—V8 | 39.02 (10) |
| V14—O12—V12 | 100.21 (17) | O5—V1—V8 | 124.08 (11) |

Table 2.4 (Continued): Selected bond angles for bpy-$V_{15}$

| Bond | angle $^{o}$ | Bond | angle $^{o}$ |
|---|---|---|---|
| O35—V1—V6 | 116.02 (16) | O18—V3—V12 | 109.11 (14) |
| O6—V1—V6 | 122.30 (10) | O21—V3—V12 | 130.07 (11) |
| O3—V1—V6 | 122.29 (11) | O14—V3—V12 | 108.43 (10) |
| O5—V1—V6 | 38.78 (11) | O1—V3—V12 | 39.02 (10) |
| O2—V1—V6 | 38.91 (10) | O7—V3—V12 | 38.78 (10) |
| V8—V1—V6 | 131.35 (3) | O18—V3—V13 | 107.06 (14) |
| O31—V2—O9 | 104.19 (18) | O21—V3—V13 | 130.00 (11) |
| O31—V2—O8 | 107.53 (18) | O14—V3—V13 | 38.63 (10) |
| O9—V2—O8 | 77.81 (14) | O1—V3—V13 | 109.17 (10) |
| O31—V2—O14 | 106.21 (18) | O7—V3—V13 | 39.57 (10) |
| O9—V2—O14 | 93.68 (14) | V12—V3—V13 | 72.70 (3) |
| O8—V2—O14 | 146.25 (14) | O13—V4—O9 | 111.95 (18) |
| O31—V2—O11 | 107.99 (18) | O13—V4—O4 | 111.96 (18) |
| O9—V2—O11 | 147.81 (14) | O9—V4—O4 | 135.41 (14) |
| O8—V2—O11 | 92.50 (14) | O13—V4—O21 | 102.41 (17) |
| O14—V2—O11 | 77.38 (14) | O9—V4—O21 | 88.87 (15) |
| O31—V2—V9 | 113.39 (16) | O4—V4—O21 | 89.13 (15) |
| O9—V2—V9 | 38.63 (9) | O13—V4—O10 | 104.14 (17) |
| O8—V2—V9 | 39.36 (10) | O9—V4—O10 | 81.15 (14) |
| O14—V2—V9 | 122.94 (10) | O4—V4—O10 | 81.16 (14) |
| O11—V2—V9 | 123.34 (10) | O21—V4—O10 | 153.46 (14) |
| O31—V2—V13 | 115.89 (16) | O13—V4—V9 | 112.22 (15) |
| O9—V2—V13 | 123.85 (10) | O9—V4—V9 | 40.56 (10) |
| O8—V2—V13 | 121.03 (11) | O4—V4—V9 | 112.85 (10) |
| O14—V2—V13 | 39.65 (9) | O21—V4—V9 | 126.03 (10) |
| O11—V2—V13 | 38.03 (10) | O10—V4—V9 | 40.66 (10) |
| V9—V2—V13 | 130.72 (4) | O13—V4—V15 | 112.01 (14) |
| O18—V3—O21 | 104.32 (17) | O9—V4—V15 | 112.92 (10) |
| O18—V3—O14 | 108.06 (18) | O4—V4—V15 | 40.68 (10) |
| O21—V3—O14 | 94.75 (15) | O21—V4—V15 | 126.45 (11) |
| O18—V3—O1 | 110.27 (18) | O10—V4—V15 | 40.56 (10) |
| O21—V3—O1 | 94.86 (16) | V9—V4—V15 | 76.68 (3) |
| O14—V3—O1 | 136.59 (14) | O22—V5—O23 | 105.2 (2) |
| O18—V3—O7 | 96.93 (17) | O22—V5—O2 | 109.15 (18) |
| O21—V3—O7 | 158.75 (14) | O23—V5—O2 | 95.93 (16) |
| O14—V3—O7 | 78.18 (14) | O22—V5—O8 | 110.54 (18) |

Table 2.5: Selected bond angles for pyridine molecules

| Bond | angle $^{o}$ | Bond | angle $^{o}$ |
|---|---|---|---|
| ∠C6—N4—H4A | 113.43(623) | ∠N1—C19—H19 | 120.24(64) |
| ∠C6—N4—C8 | 121.24(62) | ∠C18—C19—H19 | 120.22(59) |
| ∠C8—N4—H4A | 123.85(609) | ∠C18—C19—N1 | 119.54(58) |
| **TOTAL** | **358.52** | **TOTAL** | **360.00** |
| | | | |
| ∠C30—N1—C19 | 122.08(62) | ∠N2—C1—C20 | 120.18(75) |
| ∠C30—N1—H1A | 113.90(681) | ∠H1—C1—C20 | 119.94(82) |
| ∠C19—N1—H1A | 123.92(659) | ∠H1—C1—N2 | |
| 119.88(86) | | | |
| **TOTAL** | **359.90** | **TOTAL** | **360.00** |
| | | | |
| ∠C37—N5—C24 | 120.41(67) | ∠C34—C25—C14 | 121.08(61) |
| ∠H5A—N5—C24 | 126.23(485) | ∠C34—C25—H25 | 119.41(64) |
| ∠H5A—N5—C37 | 113.35(457) | ∠H25—C25—C14 | 119.51(62) |
| **TOTAL** | **359.99** | **TOTAL** | **360.00** |
| | | | |
| ∠C10—N6—H6A | 118.92(553) | ∠C11—C18—C19 | 120.53(55) |
| ∠C10—N6—C26 | 121.86(53) | ∠H18—C18—C19 | 119.89(57) |
| ∠C26—N6—H6A | 118.68(560) | ∠H18—C18—C11 | 119.58(56) |
| **TOTAL** | **359.46** | **TOTAL** | **360.00** |
| | | | |
| ∠N1—C30—C21 | 120.51(75) | ∠N2—C34—C25 | 119.95(73) |
| ∠C21—C30—H3 | 119.67(73) | ∠H34—C34—N2 | 119.85(82) |
| ∠N1—C30—H30 | 119.82(66) | ∠H34—C34—C25 | 120.20(81) |
| **TOTAL** | **360.00** | **TOTAL** | **360.00** |
| | | | |
| ∠C11—C21—C30 | 119.77(64) | ∠H20—C20—C1 | 120.55(68) |
| ∠C11—C21—H21 | 119.98(62) | ∠H20—C20—C14 | 120.75(65) |
| ∠C30—C21—H21 | 120.25(83) | ∠C1—C20—C14 | 118.71(60) |
| **TOTAL** | **360.00** | **TOTAL** | **360.01** |

Table 2.6: Selected Fractional atomic coordinates and isotropic or equivalent isotropic displacement parameters ($Å^2$)

| | *x* | *y* | *z* | *Uiso*/Ueq* | *Occ. (<1)* |
|---|---|---|---|---|---|
| V1 | 0.08750 (4) | 0.95689 (6) | 0.13328 (3) | 0.03142 (19) | |
| V2 | 0.42574 (5) | 0.92122 (6) | 0.10479 (3) | 0.03151 (18) | |
| V3 | 0.42258 (5) | 0.68782 (6) | 0.17358 (3) | 0.03128 (18) | |
| V4 | 0.38386 (5) | 0.65641 (6) | 0.06079 (3) | 0.03268 (19) | |
| V5 | 0.24359 (5) | 1.04269 (6) | 0.06052 (3) | 0.0380 (2) | |
| V6 | 0.12007 (5) | 0.87358 (7) | 0.03920 (3) | 0.0378 (2) | |
| V7 | 0.06653 (5) | 0.68894 (6) | 0.08959 (3) | 0.0384 (2) | |
| V8 | 0.17818 (5) | 0.93315 (7) | 0.22225 (3) | 0.03444 (19) | |
| V9 | 0.32888 (5) | 0.85397 (7) | 0.02191 (3) | 0.0371 (2) | |
| V10 | 0.23993 (5) | 0.55222 (6) | 0.14069 (3) | 0.03453 (19) | |
| V11 | 0.28135 (5) | 1.06783 (6) | 0.17261 (3) | 0.0376 (2) | |
| V12 | 0.27169 (5) | 0.68158 (7) | 0.22662 (3) | 0.0361 (2) | |
| V13 | 0.38898 (5) | 0.91029 (6) | 0.20460 (3) | 0.03286 (19) | |
| V14 | 0.10255 (5) | 0.72142 (7) | 0.20097 (3) | 0.0379 (2) | |
| V15 | 0.21276 (5) | 0.62137 (7) | 0.04321 (3) | 0.0378 (2) | |
| Cl1 | 0.25198 (7) | 0.81011 (10) | 0.12669 (5) | 0.0408 (3) | |
| O1 | 0.32998 (19) | 0.6044 (3) | 0.18124 (12) | 0.0351 (7) | |
| O2 | 0.1400 (2) | 0.9968 (2) | 0.07667 (12) | 0.0352 (7) | |
| O3 | 0.17040 (19) | 1.0270 (2) | 0.17141 (12) | 0.0337 (7) | |
| O4 | 0.29812 (19) | 0.5732 (2) | 0.08374 (12) | 0.0347 (7) | |
| O5 | 0.05944 (19) | 0.8392 (3) | 0.09211 (13) | 0.0377 (8) | |
| O6 | 0.09048 (18) | 0.8667 (3) | 0.18748 (12) | 0.0347 (7) | |
| O7 | 0.36487 (19) | 0.7675 (3) | 0.22409 (12) | 0.0346 (7) | |
| O8 | 0.3459 (2) | 0.9771 (3) | 0.05923 (12) | 0.0362 (7) | |
| O9 | 0.41202 (19) | 0.8024 (2) | 0.06221 (12) | 0.0329 (7) | |
| O10 | 0.2925 (2) | 0.7129 (3) | 0.02063 (12) | 0.0348 (7) | |
| O11 | 0.38099 (19) | 1.0057 (2) | 0.15496 (12) | 0.0334 (7) | |
| O12 | 0.18437 (19) | 0.6188 (3) | 0.19230 (13) | 0.0380 (8) | |
| O13 | 0.4377 (2) | 0.5910 (3) | 0.02635 (13) | 0.0427 (8) | |
| O14 | 0.44451 (18) | 0.8293 (2) | 0.15879 (12) | 0.0314 (7) | |
| O15 | 0.2384 (2) | 0.4278 (3) | 0.14893 (16) | 0.0486 (10) | |
| O16 | 0.1516 (2) | 0.5884 (3) | 0.09606 (14) | 0.0399 (8) | |
| O17 | 0.29075 (19) | 0.9578 (3) | 0.22257 (12) | 0.0360 (7) | |

Table 2.6 (Continued.) **:** Selected Fractional atomic coordinates and isotropic or equivalent isotropic displacement parameters ($Å^2$)

| | *x* | *y* | *z* | *Uiso*/Ueq* | *Occ. (<1)* |
|---|---|---|---|---|---|
| O18 | 0.4962 (2) | 0.6443 (3) | 0.20524 (13) | 0.0423 (8) | |
| O19 | 0.2215 (2) | 0.9056 (3) | 0.01823 (12) | 0.0378 (8) | |
| O20 | 0.0447 (2) | 0.6795 (3) | 0.15062 (14) | 0.0411 (8) | |
| O21 | 0.44174 (19) | 0.6387 (2) | 0.11814 (12) | 0.0333 (7) | |
| O22 | 0.2343 (2) | 1.1299 (3) | 0.02075 (15) | 0.0471 (9) | |
| O23 | 0.2643 (2) | 1.1134 (3) | 0.11047 (13) | 0.0389 (8) | |
| O24 | 0.1332 (2) | 0.7279 (3) | 0.03460 (12) | 0.0361 (7) | |
| O25 | 0.2933 (2) | 1.1756 (3) | 0.19967 (16) | 0.0494 (10) | |
| O26 | 0.0474 (2) | 0.6871 (3) | 0.24237 (15) | 0.0479 (9) | |
| O27 | 0.1949 (3) | 0.5334 (3) | 0.00436 (15) | 0.0533 (10) | |
| O28 | 0.4570 (2) | 0.9501 (3) | 0.24101 (14) | 0.0481 (9) | |
| O29 | 0.2009 (2) | 0.7871 (3) | 0.23745 (12) | 0.0372 (7) | |
| O30 | 0.0553 (2) | 0.9039 (3) | −0.00052 (15) | 0.0530 (10) | |
| O31 | 0.5118 (2) | 0.9698 (3) | 0.09319 (15) | 0.0463 (9) | |
| O32 | 0.1435 (2) | 0.9889 (3) | 0.26704 (14) | 0.0501 (9) | |
| O33 | 0.3664 (3) | 0.8771 (3) | −0.02691 (14) | 0.0554 (10) | |
| O34 | 0.2829 (2) | 0.6168 (3) | 0.27352 (15) | 0.0514 (10) | |
| O35 | 0.0077 (2) | 1.0285 (3) | 0.13730 (15) | 0.0475 (9) | |
| O36 | −0.0121 (2) | 0.6400 (3) | 0.06323 (16) | 0.0491 (10) | |
| O37 | −0.1135 (4) | 0.6058 (7) | −0.4441 (3) | 0.121 (3) | |
| O38 | 0.7027 (6) | 0.8065 (7) | 0.6089 (3) | 0.104 (3) | 0.78 |
| O39 | 0.6933 (6) | 0.8777 (7) | 0.2505 (3) | 0.114 (3) | 0.82 |
| O40 | −0.1587 (6) | 0.6045 (11) | −0.3544 (3) | 0.138 (4) | 0.78 |
| O41 | 0.6265 (5) | 0.8401 (11) | 0.1662 (4) | 0.139 (4) | 0.78 |
| O42 | 0.1349 (7) | 0.4018 (9) | −0.1470 (4) | 0.147 (4) | 0.84 |
| O43 | 0.3040 (6) | 0.4984 (11) | 0.3891 (5) | 0.137 (5) | 0.71 |

Table 2.7: Atomic displacement parameters ($Å^2$) for bpy- $V_{15}$

| | U11 | U22 | U33 | U12 | U13 | U23 |
|---|---|---|---|---|---|---|
| V1 | 0.0266 (4) | 0.0284 (4) | 0.0391 (5) | 0.0083 (3) | −0.0003 (3) | −0.0011 (3) |
| V2 | 0.0287 (4) | 0.0320 (4) | 0.0340 (4) | 0.0022 (3) | 0.0040 (3) | −0.0001 (3) |
| V3 | 0.0298 (4) | 0.0323 (4) | 0.0316 (4) | 0.0103 (3) | −0.0009 (3) | −0.0006 (3) |
| V4 | 0.0321 (4) | 0.0326 (4) | 0.0334 (4) | 0.0094 (3) | 0.0022 (3) | −0.0053 (3) |
| V5 | 0.0375 (4) | 0.0304 (4) | 0.0462 (5) | 0.0062 (3) | 0.0042 (4) | 0.0092 (4) |
| V6 | 0.0405 (5) | 0.0348 (4) | 0.0373 (5) | 0.0081 (3) | −0.0095 (4) | −0.0017 (3) |
| V7 | 0.0309 (4) | 0.0316 (4) | 0.0524 (6) | 0.0018 (3) | −0.0028 (4) | −0.0030 (4) |
| V8 | 0.0344 (4) | 0.0381 (4) | 0.0310 (4) | 0.0086 (3) | 0.0045 (3) | −0.0029 (3) |
| V9 | 0.0446 (5) | 0.0397 (4) | 0.0272 (4) | 0.0086 (3) | 0.0034 (3) | 0.0014 (3) |
| V10 | 0.0347 (4) | 0.0259 (4) | 0.0430 (5) | 0.0036 (3) | 0.0008 (3) | 0.0017 (3) |
| V11 | 0.0331 (4) | 0.0288 (4) | 0.0508 (6) | 0.0034 (3) | 0.0021 (4) | −0.0093 (4) |
| V12 | 0.0356 (4) | 0.0396 (4) | 0.0332 (5) | 0.0084 (3) | 0.0028 (3) | 0.0062 (3) |
| V13 | 0.0320 (4) | 0.0353 (4) | 0.0310 (4) | 0.0068 (3) | −0.0024 (3) | −0.0066 (3) |
| V14 | 0.0354 (4) | 0.0346 (4) | 0.0444 (5) | 0.0042 (3) | 0.0110 (4) | 0.0049 (4) |
| V15 | 0.0386 (4) | 0.0345 (4) | 0.0395 (5) | 0.0080 (3) | −0.0073 (4) | −0.0093 (4) |
| Cl1 | 0.0431 (6) | 0.0412 (6) | 0.0380 (7) | 0.0043 (5) | 0.0009 (5) | −0.0001 (5) |
| O1 | 0.0340 (17) | 0.0344 (17) | 0.0369 (19) | 0.0071 (13) | 0.0015 (14) | −0.0006 (14) |
| O2 | 0.0392 (18) | 0.0305 (16) | 0.0360 (19) | 0.0044 (13) | 0.0006 (14) | 0.0021 (14) |
| O3 | 0.0332 (16) | 0.0278 (15) | 0.040 (2) | 0.0047 (12) | 0.0010 (14) | −0.0028 (13) |
| O4 | 0.0329 (17) | 0.0314 (16) | 0.040 (2) | 0.0086 (13) | −0.0028 (14) | −0.0041 (14) |
| O5 | 0.0346 (17) | 0.0310 (16) | 0.047 (2) | 0.0044 (13) | 0.0008 (15) | −0.0029 (15) |
| O6 | 0.0294 (16) | 0.0345 (17) | 0.041 (2) | 0.0069 (13) | 0.0060 (14) | −0.0005 (14) |
| O7 | 0.0363 (17) | 0.0375 (17) | 0.0301 (18) | 0.0076 (13) | 0.0028 (14) | −0.0006 (14) |
| O8 | 0.0378 (17) | 0.0325 (16) | 0.039 (2) | 0.0058 (13) | 0.0041 (14) | 0.0036 (14) |
| O9 | 0.0334 (16) | 0.0340 (16) | 0.0315 (18) | 0.0083 (13) | 0.0049 (13) | −0.0006 (13) |
| O10 | 0.0380 (17) | 0.0373 (17) | 0.0290 (18) | 0.0075 (14) | −0.0008 (14) | −0.0074 (14) |
| O11 | 0.0325 (16) | 0.0298 (16) | 0.0381 (19) | 0.0014 (12) | 0.0038 (14) | −0.0036 (13) |
| O12 | 0.0344 (17) | 0.0357 (17) | 0.044 (2) | 0.0031 (14) | 0.0050 (15) | 0.0037 (15) |
| O13 | 0.0425 (19) | 0.049 (2) | 0.036 (2) | 0.0173 (16) | 0.0014 (15) | −0.0118 (16) |
| O14 | 0.0274 (15) | 0.0327 (16) | 0.0342 (18) | 0.0062 (12) | 0.0018 (13) | −0.0003 (13) |
| O15 | 0.050 (2) | 0.0285 (18) | 0.068 (3) | 0.0038 (15) | 0.0016 (19) | 0.0092 (17) |

Table 2.7 (Continued): Atomic displacement parameters ($Å^2$) for bpy-$V_{15}$

| | U11 | U22 | U33 | U12 | U13 | U23 |
|---|---|---|---|---|---|---|
| O16 | 0.0339 (17) | 0.0350 (17) | 0.051 (2) | 0.0003 (13) | −0.0014 (15) | −0.0003 (15) |
| O17 | 0.0333 (17) | 0.0400 (18) | 0.0348 (19) | 0.0071 (13) | 0.0024 (14) | −0.0068 (14) |
| O18 | 0.0389 (18) | 0.048 (2) | 0.039 (2) | 0.0186 (15) | −0.0052 (15) | 0.0025 (16) |
| O19 | 0.0378 (18) | 0.0388 (18) | 0.037 (2) | 0.0077 (14) | −0.0016 (15) | 0.0029 (15) |
| O20 | 0.0349 (17) | 0.0364 (18) | 0.052 (2) | 0.0013 (14) | 0.0014 (16) | 0.0000 (16) |
| O21 | 0.0361 (17) | 0.0340 (16) | 0.0297 (18) | 0.0081 (13) | −0.0004 (13) | −0.0014 (13) |
| O22 | 0.050 (2) | 0.0389 (19) | 0.053 (2) | 0.0065 (16) | 0.0024 (18) | 0.0158 (17) |
| O23 | 0.0388 (18) | 0.0337 (17) | 0.044 (2) | 0.0032 (14) | 0.0006 (15) | 0.0020 (15) |
| O24 | 0.0366 (17) | 0.0340 (17) | 0.037 (2) | 0.0062 (13) | −0.0036 (14) | −0.0055 (14) |
| O25 | 0.050 (2) | 0.0348 (19) | 0.063 (3) | 0.0012 (16) | 0.0015 (19) | −0.0163 (18) |
| O26 | 0.0400 (19) | 0.055 (2) | 0.050 (2) | 0.0011 (16) | 0.0141 (17) | 0.0120 (18) |
| O27 | 0.060 (2) | 0.043 (2) | 0.056 (3) | 0.0107 (17) | −0.015 (2) | −0.0187 (18) |
| O28 | 0.042 (2) | 0.053 (2) | 0.048 (2) | 0.0053 (16) | −0.0094 (17) | −0.0178 (18) |
| O29 | 0.0401 (18) | 0.0390 (18) | 0.0326 (19) | 0.0088 (14) | 0.0048 (14) | 0.0052 (14) |
| O30 | 0.056 (2) | 0.052 (2) | 0.049 (3) | 0.0175 (18) | −0.0176 (19) | −0.0002 (18) |
| O31 | 0.0343 (18) | 0.048 (2) | 0.057 (3) | −0.0045 (15) | 0.0064 (17) | 0.0009 (18) |
| O32 | 0.054 (2) | 0.058 (2) | 0.039 (2) | 0.0102 (18) | 0.0126 (17) | −0.0111 (18) |
| O33 | 0.065 (3) | 0.065 (3) | 0.037 (2) | 0.015 (2) | 0.0118 (19) | 0.0089 (19) |
| O34 | 0.051 (2) | 0.059 (2) | 0.045 (2) | 0.0113 (18) | 0.0062 (18) | 0.0179 (19) |
| O35 | 0.0364 (19) | 0.046 (2) | 0.059 (3) | 0.0183 (16) | −0.0015 (17) | −0.0041 (18) |
| O36 | 0.0398 (19) | 0.042 (2) | 0.064 (3) | −0.0035 (15) | −0.0107 (18) | −0.0012 (18) |
| O37 | 0.080 (4) | 0.181 (8) | 0.102 (6) | −0.001 (4) | −0.017 (4) | −0.035 (5) |
| O38 | 0.141 (7) | 0.114 (6) | 0.055 (5) | 0.027 (5) | −0.026 (5) | −0.024 (4) |
| O39 | 0.141 (7) | 0.084 (5) | 0.114 (7) | −0.020 (5) | −0.026 (6) | 0.011 (5) |
| O40 | 0.125 (7) | 0.220 (12) | 0.068 (6) | 0.072 (8) | −0.021 (5) | −0.043 (7) |
| O41 | 0.067 (5) | 0.236 (13) | 0.113 (8) | −0.002 (6) | −0.004 (5) | 0.041 (8) |
| O42 | 0.147 (8) | 0.157 (9) | 0.141 (10) | 0.019 (7) | 0.054 (7) | 0.053 (8) |
| O43 | 0.077 (6) | 0.180 (12) | 0.154 (11) | −0.006 (6) | −0.002 (6) | −0.062 (9) |
| N1 | 0.063 (3) | 0.059 (3) | 0.045 (3) | 0.005 (3) | −0.004 (2) | −0.012 (3) |
| N2 | 0.089 (5) | 0.124 (6) | 0.041 (3) | 0.004 (4) | −0.008 (3) | 0.002 (4) |
| N3 | 0.061 (3) | 0.058 (3) | 0.063 (4) | 0.004 (2) | 0.013 (3) | 0.005 (3) |
| N4 | 0.045 (3) | 0.055 (3) | 0.047 (3) | 0.026 (2) | 0.002 (2) | 0.005 (2) |

Table 2.7 (Continued.): Atomic displacement parameters ($Å^2$) for bpy-$V_{15}$

| | U11 | U22 | U33 | U12 | U13 | U23 |
|---|---|---|---|---|---|---|
| N5 | 0.081 (4) | 0.066 (4) | 0.064 (4) | 0.009 (3) | −0.015 (3) | −0.012 (3) |
| N6 | 0.038 (2) | 0.049 (3) | 0.051 (3) | 0.023 (2) | 0.006 (2) | 0.002 (2) |
| C1 | 0.072 (5) | 0.133 (7) | 0.045 (4) | 0.024 (5) | 0.019 (4) | 0.031 (4) |
| C6 | 0.060 (4) | 0.073 (4) | 0.046 (4) | 0.030 (3) | −0.014 (3) | 0.003 (3) |
| C7 | 0.069 (4) | 0.059 (4) | 0.065 (5) | 0.026 (3) | −0.008 (3) | −0.011 (3) |
| C8 | 0.141 (8) | 0.130 (8) | 0.050 (5) | 0.102 (7) | −0.033 (5) | −0.036 (5) |
| C9 | 0.071 (4) | 0.070 (4) | 0.033 (3) | 0.031 (3) | −0.012 (3) | −0.009 (3) |
| C10 | 0.037 (3) | 0.048 (3) | 0.044 (3) | 0.015 (2) | −0.001 (2) | 0.003 (2) |
| C12 | 0.046 (3) | 0.042 (3) | 0.071 (4) | 0.005 (2) | −0.001 (3) | −0.001 (3) |
| C13 | 0.053 (3) | 0.037 (3) | 0.064 (4) | 0.003 (2) | 0.006 (3) | −0.001 (3) |
| C16 | 0.062 (4) | 0.050 (3) | 0.058 (4) | 0.005 (3) | 0.011 (3) | −0.005 (3) |
| C17 | 0.047 (3) | 0.053 (3) | 0.033 (3) | 0.020 (2) | 0.004 (2) | 0.001 (2) |
| C18 | 0.043 (3) | 0.056 (3) | 0.039 (3) | −0.009 (2) | 0.002 (2) | 0.005 (2) |
| C19 | 0.053 (3) | 0.069 (4) | 0.045 (3) | −0.002 (3) | 0.008 (3) | 0.005 (3) |
| C20 | 0.056 (4) | 0.101 (5) | 0.047 (4) | 0.004 (4) | 0.007 (3) | 0.018 (4) |
| C21 | 0.077 (4) | 0.046 (3) | 0.059 (4) | −0.012 (3) | 0.008 (3) | 0.004 (3) |
| C22 | 0.069 (4) | 0.072 (4) | 0.038 (3) | 0.040 (3) | −0.007 (3) | −0.007 (3) |
| C23 | 0.047 (3) | 0.042 (3) | 0.074 (5) | 0.011 (2) | 0.011 (3) | 0.002 (3) |
| C24 | 0.063 (4) | 0.054 (4) | 0.071 (5) | 0.010 (3) | −0.018 (3) | 0.001 (3) |
| C25 | 0.068 (4) | 0.049 (3) | 0.050 (4) | −0.006 (3) | −0.004 (3) | 0.006 (3) |
| C26 | 0.068 (4) | 0.076 (4) | 0.050 (4) | 0.041 (3) | 0.012 (3) | −0.007 (3) |
| C30 | 0.075 (4) | 0.047 (3) | 0.064 (4) | −0.019 (3) | −0.008 (3) | −0.006 (3) |
| C34 | 0.085 (5) | 0.074 (5) | 0.060 (5) | −0.012 (4) | −0.017 (4) | 0.012 (4) |
| C36 | 0.065 (4) | 0.067 (4) | 0.065 (5) | 0.015 (3) | 0.006 (3) | 0.014 (3) |
| C37 | 0.084 (5) | 0.090 (6) | 0.079 (6) | 0.035 (4) | −0.004 (4) | −0.028 (5) |
| C38 | 0.108 (6) | 0.125 (7) | 0.057 (5) | 0.090 (6) | −0.048 (4) | −0.049 (5) |
| C2 | 0.037 (3) | 0.042 (3) | 0.033 (3) | 0.014 (2) | 0.000 (2) | −0.006 (2) |
| C3 | 0.031 (2) | 0.034 (2) | 0.063 (4) | 0.0004 (19) | 0.004 (2) | 0.000 (2) |
| C4 | 0.037 (3) | 0.032 (3) | 0.065 (4) | 0.000 (2) | −0.001 (2) | −0.006 (2) |
| C5 | 0.037 (3) | 0.045 (3) | 0.033 (3) | 0.011 (2) | −0.006 (2) | −0.004 (2) |
| C11 | 0.045 (3) | 0.035 (3) | 0.047 (3) | 0.008 (2) | 0.005 (2) | 0.001 (2) |
| C14 | 0.051 (3) | 0.042 (3) | 0.041 (3) | 0.015 (2) | 0.003 (2) | 0.004 (2) |

## Conclusion

Inorganic-organic hybrid material $(H_2bpy)(Hbpy)_2(V_{15}O_{36}Cl)\cdot n(H_2O)$ (n ~ 6) has been synthesized under hydrothermal conditions at 160 $^oC$. Slow cooling rate (-2.2 $^oC$/hr) and the acidic (pH = 3.5) conditions are major synthesis parameters which lead to the crystal growth of bpy-$V_{15}$. Many attempts were made to synthesize the new compound at different pH levels or fast cooling rate but were unsuccessful. The new compound forms dark green, column-like crystals. Single crystal X-ray diffraction confirms that the structure is made of self-assembled POM and bpy through H-bonding between POM anion and protonated $H_2bpy$. These units are arranged alternately to form chains along ab diagonals. Between the chains, π-π stacking of hetero-aromatic bpy rings and anion-π interactions hold the structures together further. The structure is relatively stable in nitrogen and does not lose bpy until beyond 430 $^oC$ according to TGA. The final product indicates the decomposition of the starting material. The bpy-V15 phase is the first of the kind regarding compound made of POM anion-π interactions. It contains the $Cl@\{V_{15}O_{35}\}$ cluster and three bipyridine molecules, one of which is fully pronated to extend the structure through above mentioned POM-$H_2bpy$ chain, and the other two are protonated at one side as a terminator to stop the extension of the POM-Hbpy unit. Beside the typical covalent bond between vanadium and oxygen atoms, other non-covalent bonding has been discussed in bpy-V15. The aromatic rings show a well-known π-π stacking between bpy rings. Hydrogen bonding between H···N of the bpy as well as H···O of the POM cluster has been confirmed to play an essential role in extending the structure. A third type of non-covalent bonding is the anion–π interaction which

facilitates the formation of the layer of the structure. Bond valance sum calculations and single crystal X-ray data show that the transition metal in the cluster contains two different oxidation states, nine $V^{5+}$ and six $V^{4+}$ making the total charge of the POM cluster 4-.

IR measurement confirms the presence of water by the characteristic high wavenumber of 3422 $cm^{-1}$. Also V-O and V=O bonds show distinctive peaks at 650 $cm^{-1}$and 988 $cm^{-1,}$ respectively. Thermogravimetric studies for bpy-V15 show decomposition of the compound, and weight loss of 6% at 100 $^{o}$C indicating evaporation of water, which is in good agreement with the calculated number of water molecules.

Literature Cited


1. Miras, H. N.; Yan, J.; Long, D.; Cronin, L. *Chem. Soc. Rev.* **2012**, *22*, 7403-30.

2. Queen, W.; West , J.; Hwu, S. Tran, T.; Halasyamani, P.; VanDerveer, D. *Chem. Commun.* . **2012,** *48, 1665–1667.*

3. Sheldrick, G. M. SHELX97. Programs for Crystal Structure Analysis (Release 97-2). University of Göttingen, GermanySheldrick, G. M. In Crystallographic Computing 3; (**1997**).

4. Sheldrick, G. M., Kruger, C., Goddard, R., Eds.; Oxford Univ. Press: London., **1985**; ,pp 175-189.

5. Sheldrick, G. M. In SHELXTL, Version 6.1 Structure Determination Software Programs.

6. Bruker. Analytical X-ray Systems Inc. Madison, WI, USA.**2001**.

7. Pope, M.; Müller, A. *Angew. Chem., Int. Ed.* **1991,** *30*, 34-48.

8. Queen, W.; West, J.; Hudson, J.; Hwu, S. *Inorg. Chem*. **2011**, *21*, 11064-11068.

9. Shannon, R. D. *Acta Cryst.C*. **1976**, *A32*, 751-767.

10. Gung, B.; Xue, X.; Reich, H. *J. Org. Chem*. **2005**, *70*, 3641-3644.

11. Gung, B.; Patel, M.; Xue, X. *J. Org. Chem*. **2005,** *70*, 10532-10537.

12. Wang, D.; Wang, M. *J. Am. Chem. Soc*. **2013**, *135*, 892−897.

13. Gamez, P.; Mooibroek, T.; Teat, S.; Reedij, J. *Acc. Chem. Res.* **2007,** *40*, 435–444.

14. Demeshko, S.; Dechert, S.; Meyer, F. *J. Am. Chem. Soc*. **2004**, *126*, 4508–4509.

15. Hoog, P.; Gamez, P.; Mutikainen, H.; Turpeinen, U.; Reedijk, J. *Angew. Chem. Int. Ed*. **2004**, *43*, 5815 –5817.

16. Steiner. T. *Angew. Chem. Int. Ed*. **2002**, *41*, 48-76.

17. Grabowski, S. *Chem. Phys. Lett.* **2001**, *338*, 361-366.

18. Wutkowski, A.; Evers, N.; Bensch, W. *Z. Anorg. Allg. Chem.* **2011**, *637*, 2205–2210.

19. Dorn, T.; Janiak, C.; Abu-Shandi, K. *Cryst. Eng. Comm.* **2005**, *7*, 633–641.

20. Mirzaei, M.; Eshtiagh-Hosseini, H.; Lotfian, N.; Salimi, A.; Bauzá, A.; Van Deun, R.; Decadt, R.; Barceló-Oliverb, M.; Frontera, A. *Dalton Trans*. **2014**, *43*, 1906–1916.

21. Kulikov, V.; Meyer, G. *Cryst. Growth Des.* **2013**, *13*, 2916−2927.

22. Deng, Q.; Huang, Y.; Peng, Z.; Dai, Z.; Lin, M.; Cai, T. *J. Sold State Chem.* **2013**, *200*, 60–69.

23. Hayashi, Y.; Miyakoshi, N.; Shinguchi, T.; Uehara, A. *Chem. Lett.* **2001**, *30*, 170–171.

24. Buzzoni, R.; Bordiga, S.; Ricchiardi, G.; Spoto, G.;Zecchina, A, *J. Phys. Chem*. **1995**, *99*, 11937-11951.

25. Hester, B.; Sulejmanovic, D. unpublished research, Clemson University, **2012**.

# CHAPTER THREE

# SYNTHESIS AND CHARACTERIZATION OF $Cs_4(SO_4@V_{12}As_8O_{40})$ AND $Cs_2Mn_4(S_2O_7)(SO_4)_2$, REACTION PRODUCTS IN THE ABSENCE OF SELF-ASSEMBLY OF POV-BPY HYBRID

## Introduction

As mentioned previously, polyoxometalate (POM) clusters have an unmatched range of physical and chemical properties, acting as a set of transferable building blocks that can be reliably utilized in the formation of new materials[1, 2]. New POM-bpy hybrid can be synthesized, as demonstrated by the formation of a new POV-bpy discussed in chapter two, through self-assembly and the formation of non-conventional bonding such as H-bonding, as well as anion-π and π-π interactions. In this chapter, we will describe the synthesis of two new compounds arising from the reactions that were designed to explore optimal conditions for the synthesis of new POV-bpy hybrids. The new compounds, namely $Cs_4(SO_4@V_{12}As_8O_{40})$ **1** and $Cs_2Mn_4(S_2O_7)(SO_4)_2$ **2**, were synthesized in the reactions employing the same $Cs_5V_{14}As_8O_{42}Cl$ precursor but showing no evidence for the formation of POV-bpy hybrid structures. Instead, **1** is a new POV salt containing a "transformed" polyoxovanadate cluster and **2** a condensed low-dimensional framework possessing little relevance to POM. The formation of these compounds can be considered conceivably upon the decomposition of POM-containing precursor salt. Nevertheless, these limited observations, although negative, provide some insights for the future research of optimal conditions under which new POV-bpy hybrids might exist through self-assembly.

$Cs_4(SO_4@V_{12}As_8O_{40})$ **1** and $Cs_2Mn_4(S_2O_7)(SO_4)_2$ **2** were synthesized similarly in acidic solutions under hydrothermal conditions. The original reactions that yielded the new POV-bpy hybrid, $(H_2bpy)(Hbpy)_2(V_{15}O_{36}Cl)\cdot n(H_2O)$ as described in chapter two, were selectively modified to explore optimal conditions for the synthesis of this and any new POV-bpy hybrids. Instead of forming hybrid structure containing employed POV cluster anion, $\{Cl@V_{14}As_8O_{42}\}^{5-}$, **2** was isolated suggesting a total decomposition of the employed POV cluster in the precursor. Compound **1**, however, was a new POV salt containing a different cluster $\{SO_4@V_{12}As_8O_{40}\}^{4-}$ that encapsulates a sulfate unit from the anion of employed manganese sulfate salt, $MnSO_4\cdot nH_2O$. It suggests that the $\{Cl@V_{14}As_8O_{42}\}^{5-}$ Keggin cluster is subject to (possibly partial) decomposition under the employed conditions followed by the formation of a new, $\{SO_4@V_{12}As_8O_{40}\}^{4-}$. The following sections report and discuss the reaction conditions that might lead to decomposition. Hopefully, from understanding these additional variables identified from the results of failed reactions, critical parameters to the future success in exploring new POM-organic hybrids by design can be eventually achieved.

## Synthetic Procedure

The previously synthesized $Cs_5V_{14}As_8O_{42}Cl$ salt was used as the source of the POV anion throughout this study.[3] As mentioned, $Cs_5V_{14}As_8O_{42}Cl$ is a water-soluble salt containing Cl-centered POV anionic cluster $\{Cl@V_{14}As_8O_{42}\}^{5-}$. The purpose of original reactions, in which the compounds **1** and **2** were formed, was two-fold: 1) to seek optimal conditions for the formation of previously discussed $(H_2bpy)(Hbpy)_2(V_{15}O_{36}Cl)\cdot n(H_2O)$ hybrid, and 2) to additionally explore possible conditions for the formation of metal-

linked POM–metal–organic hybrids. In a typical reaction, the reactants $MnSO_4 \cdot nH_2O$, $Cs_5V_{14}As_8O_{42}Cl$ and 4,4'-bipridine were loaded in mole ratio of 1:1:10, respectively. The change of manganese salt from $Mn(OAc)_2$ used in the previous synthesis to $MnSO_4 \cdot nH_2O$ was for the sake of exploring the effect that manganese salt may have for the formation POMOF structures. While no POMOF has ever been discovered, we do realize that in order to synthesize POV-bpy, the inclusion of these manganese salts is necessary and without which no POV-bpy was observed. Nevertheless, the solutions by the dissolution of $Cs_5V_{14}As_8O_{42}Cl$ and $MnSO_4 \cdot nH_2O$ in 5ml deionize water and 4,4'-bipridine in 5 ml ethanol were prepared separately prior mixing. The pH of the mixed solution was then adjusted drop-by-drop to 3.5 by adding HCl (2 M). The mixture briefly stirred for 1 min before transferred to 20 mL Teflon-lined hydrothermal container.

In addition to substituting manganese salt for the purpose of looking for new phases and revealing the role of metal ion, the reaction conditions with regard to heating and cooling processes were also altered. The reaction that yielded **1** was heated to 160°C for an hour and isothermed for two days under autogenous pressure. The furnace was programed to cool down to room temperature over 20 h. This reaction used longer heating but faster cooling compared to 15 h of isotherm and 60 h of cooling in the previous attempt for the synthesis of POM-bpy hybrid discussed in Chapter two. A longer isotherm was chosen in hopes to extend nucleation and a quicker cooling to avoid a possible dissolution of the new product at low temperature. Solid products were filtered and washed using deionized water via suction filtration method. Black / dark green column crystals were selected under an optical microscope and mounted for single crystal

X-ray diffraction (SXRD) study. The overall reaction yielded a small amount of solid product, thus no PXRD investigation was done, and less than 10% of which were column crystals of **1**.

As to the reaction resulted in compound **2**, the synthesis procedures and reactants were kept the same as the reaction stated above. But, the heating program was varied slightly. Reactants were heated to 160°C for one hour but only isothermed for 15 h under autogenous pressure. Then the furnace was programed for slow cooling to room temperature over 50 h, 2.5× slower than the rate in the former. Slow cooling yielded increased crystals yield. Unfortunately, neither crystals of **1** nor product(s) containing POM cluster were observed. After washing with deionized water, black chunk crystals were isolated under an optical microscope and mounted for SXRD study. It is noted that only a relatively small yield of solid product was retrieved and in which, only few black chucks and small cube-like crystals (ca. 60% by volume of the solid product) were observed under optical microscope. It is worth here to mention that before set the discussed reaction conditions for compounds **1** and **2**, the reaction was set to exactly same conditions of **bpy-$V_{15}$** ( 160 $^{o}$C for 15h and cooled down over 60h) and only change the metal salt to $MnSO_4$ but there are no evidence for crystal formation.

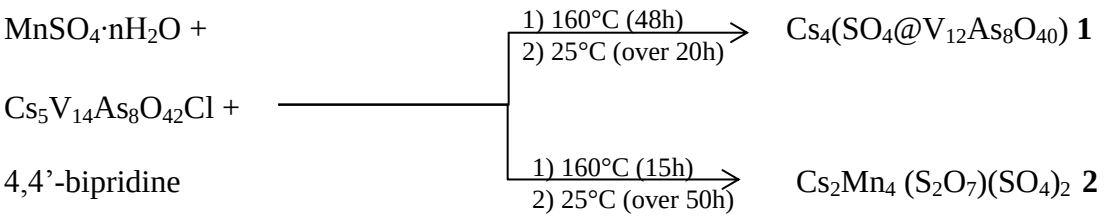


Structure Determination

The SXRD data were collected at room temperature on a four-circle Rigaku AFC8 diffractometer equipped with a Mercury CCD area detector and Mo Kα (λ= 0.71073 Å) radiation. An empirical multiscan absorption correction was applied using *REQAB*, a subroutine of the *CrystalClear* software package. Refinement of the crystal structures using a full-matrix, least-squares technique was performed employing the SHELXTL package software (version 6.1).[4-7] The data crystals were mounted on glass fibers with epoxy for the data collection of X-ray diffraction experiments.

## Results and Discussion of $Cs_4(SO_4@V_{12}As_8O_{40})$ **1**

Compound **1** crystallizes in the tetragonal crystal system, space group *I*4/*m* (No. 87), with the unit cell dimensions of a = b = 15.211 (2) Å, c = 11.687(2) Å and V = 2704.1 (8) $A^3$, see more details regarding the crystallographic date in Table 3.2**.** Single crystal X-ray data reveal that the structure of **1** contains Keggin-type POMs that adopt a general formula $[XM_{12}O_{40}]^{x-}$.[8,12] Each cluster is centered around the corners as well as the body center of the unit cell, see Figure. 3.1. The cluster anion $\{SO_4@V_{12}As_8O_{40}\}^{4-}$ adopts $D_{4h}$, symmetry. Each cluster is made of twelve $VO_5$ square pyramidal units and four $As_2O_5$ dimers. Through sharing common oxygen atoms, it forms a hollow sphere where the $SO_4^{2-}$ anion resides. Specifically, the cluster can be viewed as made of the $V_{12}O_{36}$ cage (Figure 3.2) in which four $V_3O_{11}$ trimers are related by four-fold rotational symmetry and linked through sharing corner oxygen, O6. Each trimer is made of three $VO_5$ square pyramids *via* sharing opposite edges of the square plane. The dimeric $As_2O_5$

units bridge the $V_3O_{11}$ trimers through sharing common oxygen atoms, O2 and O3, see Figure. 3.2.

From the formula mentioned above, it is obvious that the cluster is a -4 anion indicating the contribution of 54 positive charges from V atoms as the oxidation states of $As^{3+}$ and $SO_4^{2-}$ are respectively assigned. On the basis of bond-valence sum calculations for the vanadium atoms,[9] the total calculated positive charge of vanadium is 55.1 (see Table 3.1), which is the close as the expected value corresponding to four 4+ (for V1) and eight 5+ (for V2) vanadium cations. This close match confirms the structure composition despite of the relatively large R values.[10]

The POM cluster skeleton consists of twelve V=O vanadyl bonds ranging from 1.576(12) to 1.613(15) Å. Sixteen of non-vanadyl oxygen atoms, O2 and O3, of the anion bridge two V atoms, V1 and V2, of the $V_3O_{11}$ trimer and one As of the $As_2O_5$ unit. The remaining eight, O6, bridge two V atoms with the bond lengths ranging from 1.839(12) ~ 2.03(8) Å of the basal V−O bonds. $AsO_3$ unit also connect the cluster shell where each As bonded to oxygen with the range of bond distances between 1.761(12) and 1.776(7) Å. Inside the As-O-V cage**,** the encapsulated $SO_4^{-2}$ unit is disordered with respect to the oxygen atoms which are shared with half of the eight V2 atoms at any given moment and statistically 50% of the time with V1. In any case, the averaged S-O bond length 1.58(3) Å is in good agreement with the expected sum of Shannon crystal radii 1.48 Å. In addition, the disordered $SO_4$ unit forms a distorted tetrahedron squashing along two-fold axis with the ∠O−S−O angles, 85.1° and 180.02° (Table 3.5), largely deviating from the tetrahedral angle 109.5°.

Moving toward outside the cluster, each Cs is coordinating to eight oxygen atoms of the neighboring clusters. More specifically, each $Cs^{+}$ cation interlink two clusters through these Cs-O bonds along the c axis, see Figure. 3.3. That is to say, Cs-O interaction is significant regarding the extension of the structure **1** in two dimensions as shown in Figure 3.3. The bond distances of Cs–O range from 2.96~3.37 Å, which is comparable with 3.08 Å, the sum of Shannon crystal radii of 8-coordinate $Cs^{1+}$ and $O^{-2}$ 1.88 and 1.2 Å, respectively.[11]

The EDX result that shows the absence of Cl atom in this compound provide an ultimate confirmation for the contents of the crystal V, O, S, As and Cs, as shown in Figure 3.4.

The solubility of **1** was examined for several different types of solvents, and the results show that it is insoluble in any of the polar solvents examined, *i.e.*, water, ethanol, acetone, DMF and acetonitrile.

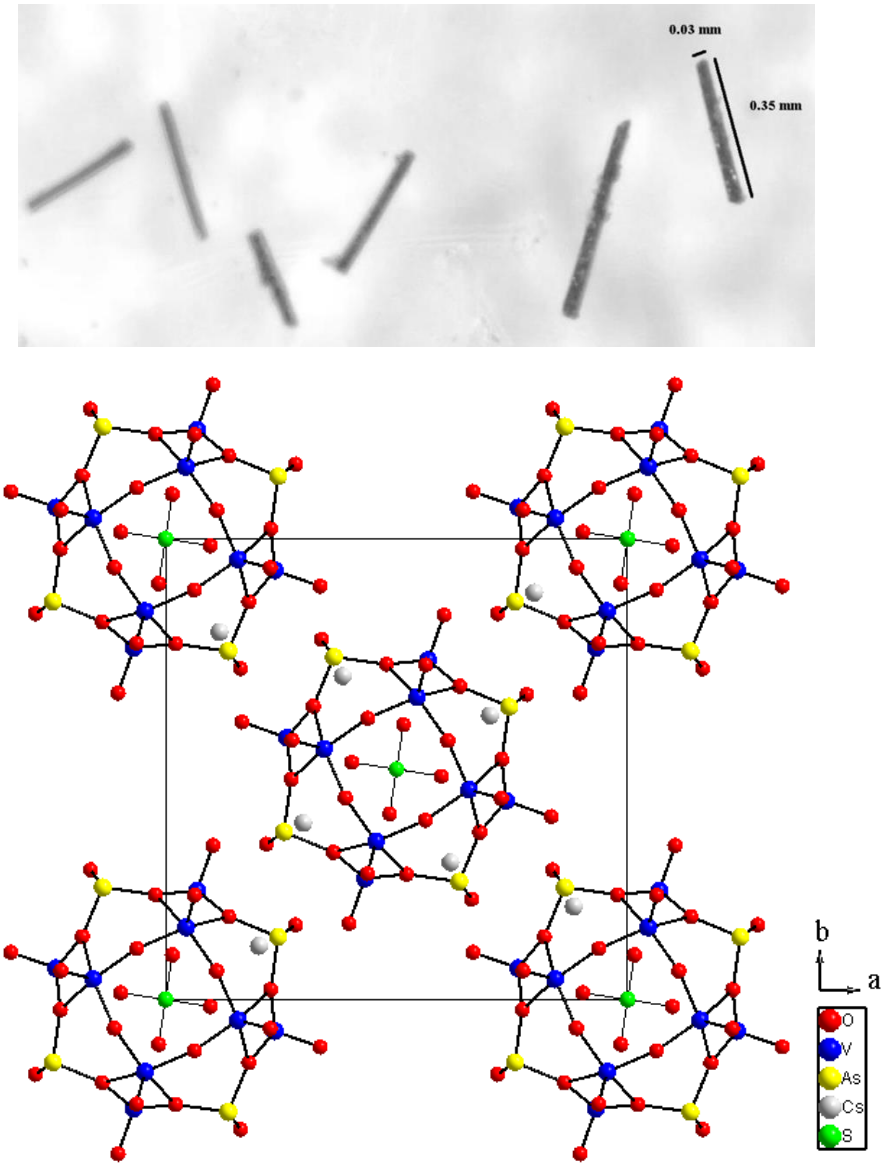


Figure 3.1: Selected crystal of **1** showing thin column/needle morphology (top). Partial structure projected along c-axis showing the unit cell of **1**. Cs-O bond is not shown for clarity. The view also shows the $SO_4$ unit encapsulated in the center of cluster (bottom).

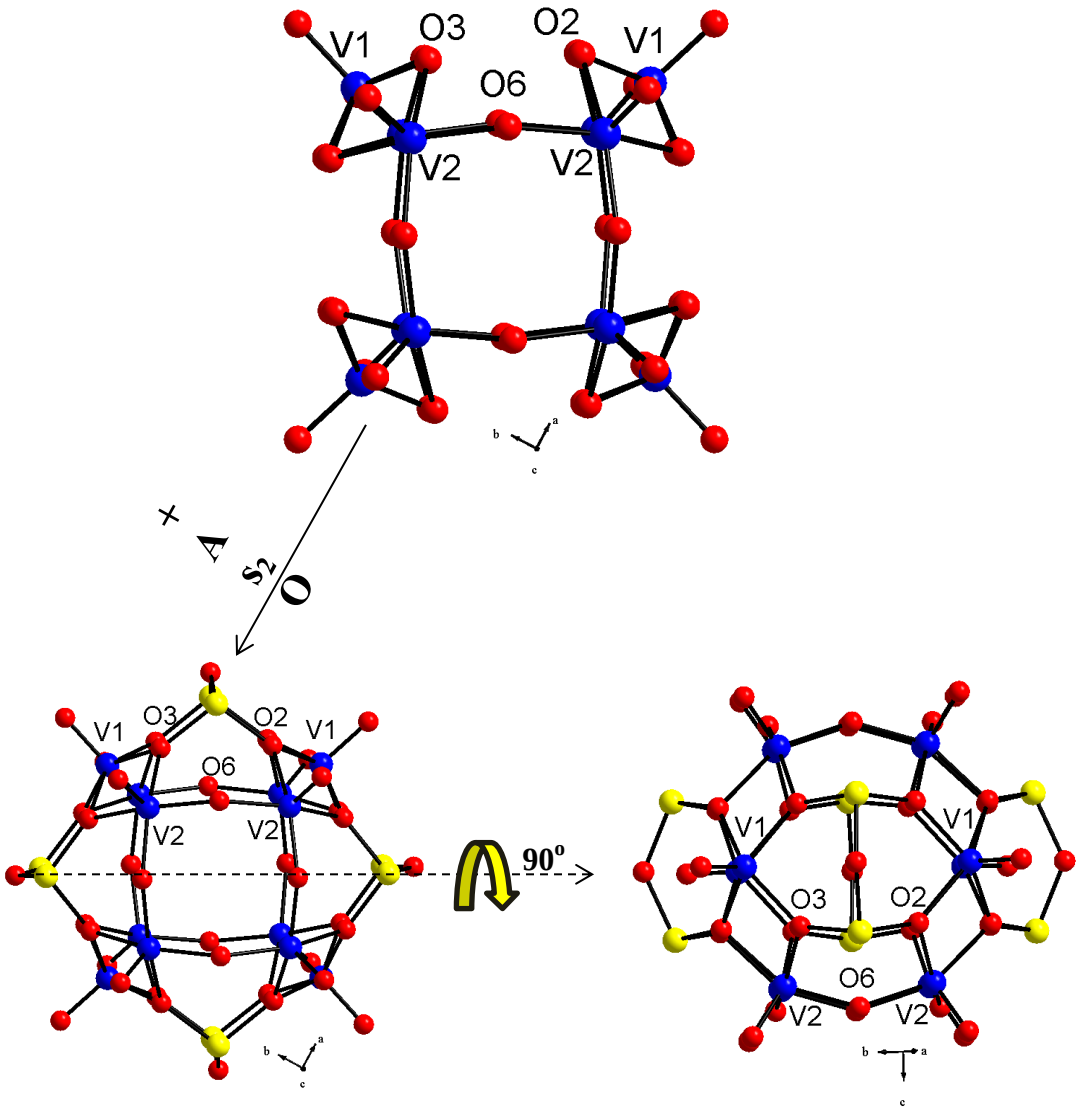


Figure 3.2: Perspective view of the cluster skeleton made of twelve connected $VO_5$ units (top). Schematically, after inserting $As_2O$ units, the cluster form the complete skeleton (bottom left) which shows $D_{4h}$ symmetry. For the structure description, a different representation showing the cluster skeleton viewed along the two-fold axis (bottom right).

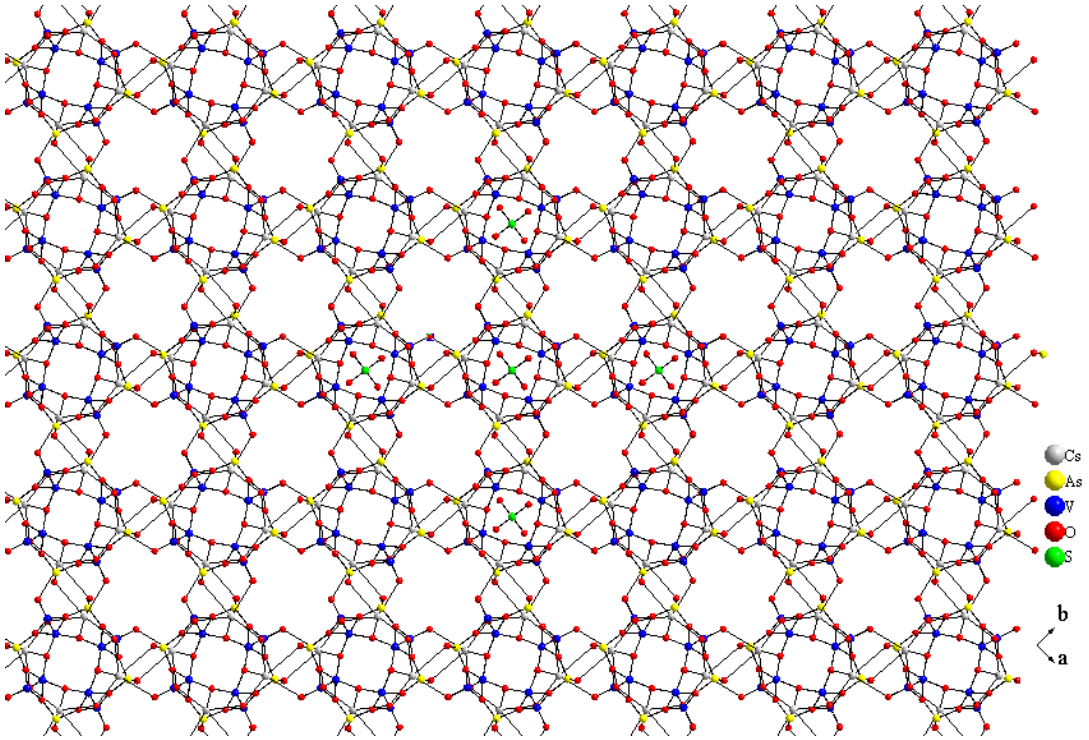


Figure 3.3: Perspective view of partial structure of **1** along the c-axis showing voids created by four neighboring cluster units which are interlined through Cs-O bonds, see text.

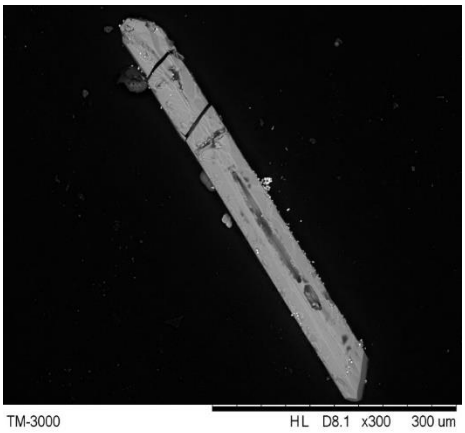


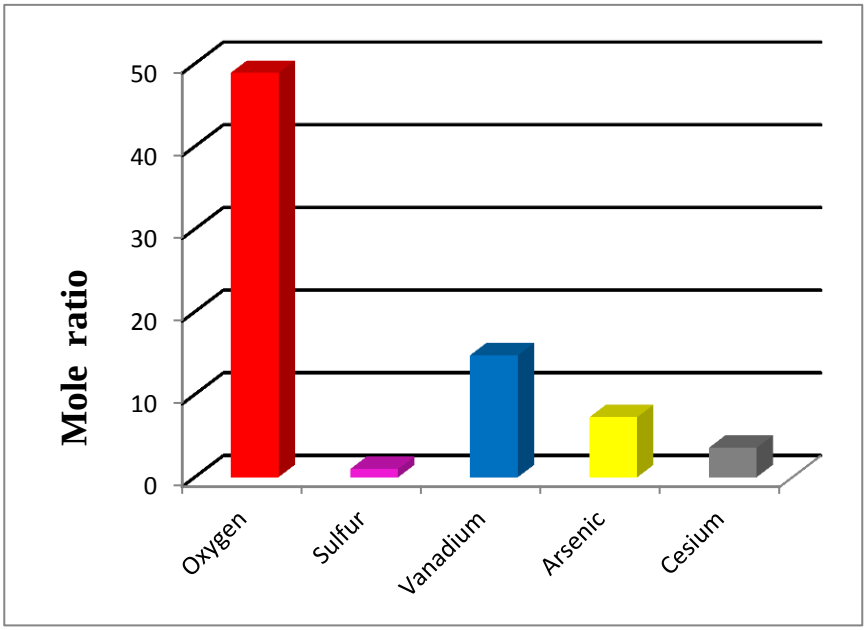


Figure 3.4: Energy dispersive X-ray (EDX) analysis for **1** showing the absence of Cl in the structure.

Table 3.1: Calculated bond valance sum for vanadium atoms in **1**

| **V1 -O distances** | 4+ | 5+ | **V2 - O distances** | 4+ | 5+ |
|---|---|---|---|---|---|
| 1.576 | 1.754 | 1.847 | 1.613 | 1.588 | 1.671 |
| 1.980 | 0.589 | 0.620 | 1.839 | 0.862 | 0.907 |
| 1.980 | 0.589 | 0.620 | 1.848 | 0.841 | 0.885 |
| 1.992 | 0.570 | 0.600 | 1.992 | 0.570 | 0.600 |
| 1.992 | 0.570 | 0.600 | 2.027 | 0.519 | 0.546 |
| 2.324 | 0.232 | 0.245 | 2.560 | 0.123 | 0.129 |
| **4** | 4.304 | 4.531 | **5** | 4.502 | 4.739 |

$(4\ V^{4.304+}) + (8\ V^{4.739+}) = 12\ V^{55.1+}$

$r_{0:}$ $V^{4+}$ 1.784
$V^{5+}$ 1.803

Table 3.2: Crystallographic data for $Cs_4(SO_4@V_{12}As_8O_{40})$ **1**

| | |
|---|---|
| Empirical formula | $Cs_4(SO_4@V_{12}As_8O_{40})$ |
| Formula weight (amu) | 2478.33 |
| Color/shape | Dark green, column |
| Crystal system | Tetragonal |
| Space group, Z | *I*4/*m* (87), 2 |
| T, °K | 293 |
| a (Å) | 15.211 (2) |
| b (Å) | 15.211(2) |
| c (Å) | 11.687(2) |
| ß = α = γ ° | 90 |
| Cell volume Å3 | 2704.1 (8) |
| Density, calcd ( g/cm3) | 2.546 |
| μ (Mo Kα), $mm^{-1}$ | 6.21 |
| $F_{000}$ | 1920 |
| Data/restraints/parameters | 8380/0/95 |
| Final R1 / wR2[I > 2σ(I)] | 0.112/0.3275 |
| R1/wR2 (all data) | 0.1222/0.3055 |
| GOF | 2.600 |

Table 3.3: Atomic parameters and isotropic or equivalent isotropic displacement parameters ($Å^2$) for **1**

| | x | y | z | Uiso*/Ueq | Occ. (<1) |
|---|---|---|---|---|---|
| Cs1 | 0.38331 (12) | 0.70215 (11) | 0 | 0.0513 (8) | |
| As1 | 0.36421 (11) | 0.74376 (12) | −0.36048 (15) | 0.0396 (8) | |
| V1 | 0.2369 (2) | 0.9314 (2) | 0 | 0.0285 (10) | |
| V2 | 0.54454 (15) | 0.65683 (16) | −0.2587 (2) | 0.0294 (9) | |
| O1 | 0.3377 (11) | 0.7816 (11) | −0.5000 | 0.042 (4) | |
| O5 | 0.5630 (7) | 0.7265 (7) | −0.1574 (10) | 0.038 (3) | |
| O3 | 0.3199 (9) | 0.6367 (8) | −0.3760 (11) | 0.047 (3) | |
| O2 | 0.4782 (7) | 0.7278 (9) | −0.3773 (10) | 0.047 (3) | |
| O6 | 0.4379 (7) | 0.6108 (8) | −0.2125 (12) | 0.048 (3) | |
| O4 | 0.3347 (9) | 0.8974 (13) | 0 | 0.053 (5) | |
| S1 | 0 | 1 | −0.5000 | 0.038 (3) | |
| O21 | 0.514 (5) | 0.598 (3) | −0.460 (4) | 0.11 (3) | 0.35(6) |

Table 3.4: Selected bond distances for **1**

| Bond | distances (A) | Bond | distances (A) |
|---|---|---|---|
| Cs1—O6 | 2.964 (13) | V2—O6$^{viii}$ | 1.839 (12) |
| Cs1—O6$^{i}$ | 2.964 (13) | V2—O6 | 1.848 (12) |
| Cs1—O4 | 3.060 (19) | V2—O3$^{viii}$ | 1.992 (12) |
| Cs1—O5$^{ii}$ | 3.264 (11) | V2—O2 | 2.027 (13) |
| Cs1—O5$^{iii}$ | 3.264 (11) | V2—V1$^{ix}$ | 3.093 (3) |
| Cs1—O5 | 3.315 (12) | V2—Cs1$^{x}$ | 3.906 (3) |
| Cs1—O5$^{i}$ | 3.315 (12) | O1—As1$^{xi}$ | 1.776 (7) |
| Cs1—O1$^{iv}$ | 3.371 (17) | O1—Cs1$^{iv}$ | 3.371 (17) |
| Cs1—Cl2 | 3.5505 (18) | O5—Cs1$^{x}$ | 3.264 (11) |
| Cs1—V2$^{ii}$ | 3.906 (3) | O3—V1$^{iv}$ | 1.980 (12) |
| Cs1—V2$^{iii}$ | 3.906 (3) | O3—V2$^{ii}$ | 1.992 (12) |
| Cs1—V2 | 3.953 (3) | O2—V1$^{ix}$ | 1.992 (12) |
| As1—O2 | 1.761 (12) | O6—V2$^{ii}$ | 1.839 (12) |
| As1—O3 | 1.772 (11) | S1—O21$^{xii}$ | 1.58 (3) |
| As1—O1 | 1.776 (7) | S1—O21$^{xiii}$ | 1.58 (3) |
| As1—Cs1$^{iv}$ | 4.185 (2) | S1—O21 | 1.58 (3) |
| V1—O4 | 1.576 (15) | S1—O21$^{ii}$ | 1.58 (3) |
| V1—O3$^{iv}$ | 1.980 (12) | S1—O21$^{xiv}$ | 1.58 (3) |
| V1—O3$^{v}$ | 1.980 (12) | S1—O21$^{xi}$ | 1.58 (3) |
| V1—O2$^{vi}$ | 1.992 (12) | S1—O21$^{viii}$ | 1.58 (3) |
| V1—O2$^{vii}$ | 1.992 (12) | S1—O21$^{xv}$ | 1.58 (3) |
| V1—O21$^{vii}$ | 2.31 (4) | O21—O21$^{xi}$ | 0.92 (9) |
| V1—O21$^{vi}$ | 2.31 (4) | O21—V1$^{ix}$ | 2.31 (4) |
| V1—V2$^{vii}$ | 3.093 (3) | V2—O5 | 1.613 (11) |
| V1—V2$^{vi}$ | 3.093 (3) | | |

Table 3.5: Selected bond angles for **1**

| Bond | angle$^{o}$ | Bond | angle$^{o}$ |
|---|---|---|---|
| O2—As1—O3 | 103.7 (7) | O2$^{vi}$—V1—V2$^{vii}$ | 123.2 (4) |
| O2—As1—O1 | 99.5 (7) | O2$^{vii}$—V1—V2$^{vii}$ | 40.1 (4) |
| O3—As1—O1 | 96.8 (6) | O21$^{vii}$—V1—V2$^{vii}$ | 54.3 (11) |
| O4—V1—O3$^{iv}$ | 103.9 (6) | O21$^{vi}$—V1—V2$^{vii}$ | 77.3 (10) |
| O4—V1—O3$^{v}$ | 103.9 (6) | O4—V1—V2$^{vi}$ | 114.23 (7) |
| O3$^{iv}$—V1—O3$^{v}$ | 94.1 (7) | O3$^{iv}$—V1—V2$^{vi}$ | 123.9 (4) |
| O4—V1—O2$^{vi}$ | 107.0 (6) | O3$^{v}$—V1—V2$^{vi}$ | 39.0 (3) |
| O3$^{iv}$—V1—O2$^{vi}$ | 149.2 (6) | O2$^{vi}$—V1—V2$^{vi}$ | 40.1 (4) |
| O3$^{v}$—V1—O2$^{vi}$ | 78.7 (5) | O2$^{vii}$—V1—V2$^{vi}$ | 123.2 (4) |
| O4—V1—O2$^{vii}$ | 107.0 (6) | O21$^{vii}$—V1—V2$^{vi}$ | 77.3 (10) |
| O3$^{iv}$—V1—O2$^{vii}$ | 78.7 (5) | O21$^{vi}$—V1—V2$^{vi}$ | 54.3 (11) |
| O3$^{v}$—V1—O2$^{vii}$ | 149.2 (6) | V2$^{vii}$—V1—V2$^{vi}$ | 131.48 (14) |
| O2$^{vi}$—V1—O2$^{vii}$ | 92.1 (7) | O5—V2—O6$^{viii}$ | 101.8 (6) |
| O4—V1—O21vii | 168.3 (9) | O5—V2—O6 | 100.8 (6) |
| O3$^{iv}$—V1—O21$^{vii}$ | 69.2 (18) | O6$^{viii}$—V2—O6 | 95.7 (8) |
| O3$^{v}$—V1—O21$^{vii}$ | 86.4 (11) | O5—V2—O3$^{viii}$ | 105.4 (6) |
| O2$^{vi}$—V1—O21$^{vii}$ | 80.4 (18) | O6$^{viii}$—V2—O3$^{viii}$ | 87.5 (6) |
| O2$^{vii}$—V1—O21$^{vii}$ | 63.0 (12) | O6—V2—O3$^{viii}$ | 152.4 (6) |
| O4—V1—O21$^{vi}$ | 168.3 (9) | O5—V2—O2 | 103.8 (5) |
| O3$^{iv}$—V1—O21$^{vi}$ | 86.4 (11) | O6$^{viii}$—V2—O2 | 153.0 (6) |
| O3$^{v}$—V1—O21$^{vi}$ | 69.2 (18) | O6—V2—O2 | 88.0 (5) |
| O2$^{vi}$—V1—O21$^{vi}$ | 63.0 (12) | O3$^{viii}$—V2—O2 | 77.6 (5) |
| O2$^{vii}$—V1—O21$^{vi}$ | 80.4 (18) | O5—V2—V1$^{ix}$ | 113.0 (4) |
| O21$^{vii}$—V1—O21$^{vi}$ | 23 (2) | O6$^{viii}$—V2—V1$^{ix}$ | 120.7 (5) |
| O4—V1—V2$^{vii}$ | 114.23 (7) | O6—V2—V1$^{ix}$ | 121.3 (5) |
| O3$^{iv}$—V1—V2$^{vii}$ | 39.0 (3) | O3$^{viii}$—V2—V1$^{ix}$ | 38.7 (3) |
| O3$^{v}$—V1—V2$^{vii}$ | 123.9 (4) | O2—V2—V1$^{ix}$ | 39.3 (3) |

Table 3.5 (Continued): Selected bond angles for **1**

| Bond | angle $^{o}$ | Bond | angle$^{o}$ |
|---|---|---|---|
| As1$^{xi}$—O1—As1 | 133.3 (11) | O21—S1—O21$^{xi}$ | 34 (3) |
| As1—O3—V1$^{iv}$ | 136.2 (7) | O21$^{ii}$—S1—O21$^{xi}$ | 94.9 (10) |
| As1—O3—V2$^{ii}$ | 120.6 (7) | O21$^{xiv}$—S1—O21$^{xi}$ | 180.000 (3) |
| V1$^{iv}$—O3—V2$^{ii}$ | 102.3 (5) | O21$^{xii}$—S1—O21$^{viii}$ | 180.0 (10) |
| As1—O2—V1$^{ix}$ | 138.6 (7) | O21$^{xiii}$—S1—O21$^{viii}$ | 94.9 (9) |
| As1—O2—V2 | 119.2 (6) | O21—S1—O21$^{viii}$ | 85.1 (9) |
| V1$^{ix}$—O2—V2 | 100.7 (5) | O21$^{ii}$—S1—O21$^{viii}$ | 146 (3) |
| V2$^{ii}$—O6—V2 | 144.1 (8) | O21$^{xiv}$—S1—O21$^{viii}$ | 85.1 (10) |
| O21$^{xii}$—S1—O21$^{xiii}$ | 85.1 (9) | O21$^{xi}$—S1—O21$^{viii}$ | 94.9 (9) |
| O21$^{xii}$—S1—O21 | 94.9 (10) | O21$^{xii}$—S1—O21$^{xv}$ | 146 (3) |
| O21$^{xiii}$—S1—O21 | 180.0 (10) | O21$^{xiii}$—S1—O21$^{xv}$ | 85.1 (10) |
| O21$^{xii}$—S1—O21ii | 34 (3) | O21—S1—O21xv | 94.9 (9) |
| O21$^{xiii}$—S1—O21$^{ii}$ | 94.9 (9) | O21$^{ii}$—S1—O21xv | 180 (3) |
| O21—S1—O21ii | 85.1 (10) | O21$^{xiv}$—S1—O21$^{xv}$ | 94.9 (9) |
| O21$^{xii}$—S1—O21$^{xiv}$ | 94.9 (9) | O21$^{xi}$—S1—O21$^{xv}$ | 85.1 (9) |
| O21$^{xiii}$—S1—O21$^{xiv}$ | 34 (3) | O21$^{viii}$—S1—O21$^{xv}$ | 34 (3) |
| O21—S1—O21$^{xiv}$ | 146 (3) | O21$^{xi}$—O21—S1 | 73.0 (17) |
| O21$^{ii}$—S1—O21$^{xiv}$ | 85.1 (9) | O21$^{xi}$—O21—V1$^{ix}$ | 78.5 (10) |
| O21$^{xii}$—S1—O21$^{xi}$ | 85.1 (9) | S1—O21—V1$^{ix}$ | 149 (2) |
| O21$^{xiii}$—S1—O21$^{xi}$ | 146 (3) | | |

Symmetry codes:
(i) x, y, −z; (ii) −y+1, x, z; (iii) −y+1, x, −z; (iv) −x+1/2, −y+3/2, −z−1/2; (v) −x+1/2, −y+3/2, z+1/2; (vi) y−1/2, −x+3/2, z+1/2; (vii) y−1/2, −x+3/2, −z−1/2; (viii) y, −x+1, z; (ix) −y+3/2, x+1/2, z−1/2; (x) y, −x+1, −z; (xi) x, y, −z−1; (xii) −y+1, x, −z−1; (xiii) −x+1, −y+1, −z−1; (xiv) −x+1, −y+1, z; (xv) y, −x+1, −z−1; (xvi) −x+1, −y+1, −z.

Results and Discussion of $Cs_2Mn_4(S_2O_7)(SO_4)_2$ **2**

Compound **2** crystallizes in the monoclinic crystal system, space group $P2_1/c$ (No. 14) with the unit cell dimensions of a = 10.637(2) Å, b = 6.721(13) Å, c = 10.129(2) Å, β = 98.96(3)$^o$, V = 715.3(2) Å$^3$, see Table 3.6 with summarized crystallographic data for **2.** From the single crystal X-ray data, the compound can be considered adopting two-dimensional slab structure with the $[Mn_4(S_2O_7)(SO_4)_2]^{2-}$ slabs propagating along the *bc* plane of the monoclinic cell, see Fig. 3.5 (bottom). Bond valence sum calculations show the oxidation state of two Mn atoms is in divalent state, see Table 3.7. Mn1 is coordinated to 5 oxygen atoms forming square pyramidal geometry. The bond distance of Mn1-O is ranging from 2.094(3) Å to 2.309(3) Å which is in good agreement with 2.1 Å, the sum of Shannon crystal radii of $Mn^{2+}$ (0.89 Å) and $O^{2-}$ (1.21 Å).[11] Mn2 is coordinated to 6 oxygen atoms with octahedral geometry. Bond distance of Mn2-O are in the range of 2.094(3) ~ 2.309 Å, which is comparable to the sum of the Shannon crystal radii for 6–coordinate $Mn^{2+}$ ion and 5–coordinate $Mn^{2+}$ with $O^{2-}$, 2.18 and 2.10 Å, respectively. The angles ∠O–Mn–O of the octahedral is deviated from the ideal value 90$^o$ where four ∠O–Mn–O range from 89.03(9)$^o$ to 97.87(9)$^o$ for the square plane, and the second four with the axial O range from 84.11(10)$^o$ to 90.57 (90)$^o$. The two Mn(s) are sharing the common edge of polyhedra to extend along b. Since the $MnO_6$ and $MnO_5$ unites are distorted due to possibly the $Mn^{2+}$–$Mn^{2+}$ repulsion through the shared edge, the ∠Mn–O–Mn bond angles are greater than 90°. The ∠Mn–O–Mn bond angles are 95.81(5)° while for ∠O–Mn–O are 84.31(7)°. Tables 3.10~11 lists some selected bond distance and angles for **2.**

The structure contains two different sulfur atoms, S1 of $SO_4$ and S2 of $S_2O_7$. According to BVS, Table 3.7, S1 and S2 have the oxidation state of 5+ which is unusual for the formal oxidation state of sulfur. The common oxidation state, however, is either 4+ or 6+. This phenomenon suggests a possible delocalization of the charges through the Mn-O chain giving the oxidation state of $S^{5+}$. Nevertheless, it accounts for a charge balanced chemical formula $Cs_2Mn_4(S_2O_7)(SO_4)_2$ with the formal charges of $Cs^+$ and $Mn^{2+}$. The $S_2O_7$ units connecting the slabs form a linear geometry with the two S atoms sharing a common oxygen atom in equal distance O-S 1.579(9)Å, Figure 3.6 (top left). The bond angles for ∠O–S–O range from 103.77 (11)° to 114.02 (14)° while bond angle for ∠S–O–S is 180°. This sulfate unit in the molecule has a pseudo $D_{3V}$ symmetry as shown in Figure 3.6 (top right). The Cs-O distances ring of 3.131(2) ~ 3.580(3) Å , are a bit long compared to the sum of the Shannon crystal radii, of 11-coordinate Cs+ (1.99Å) and O2– (1.22Å).[11]

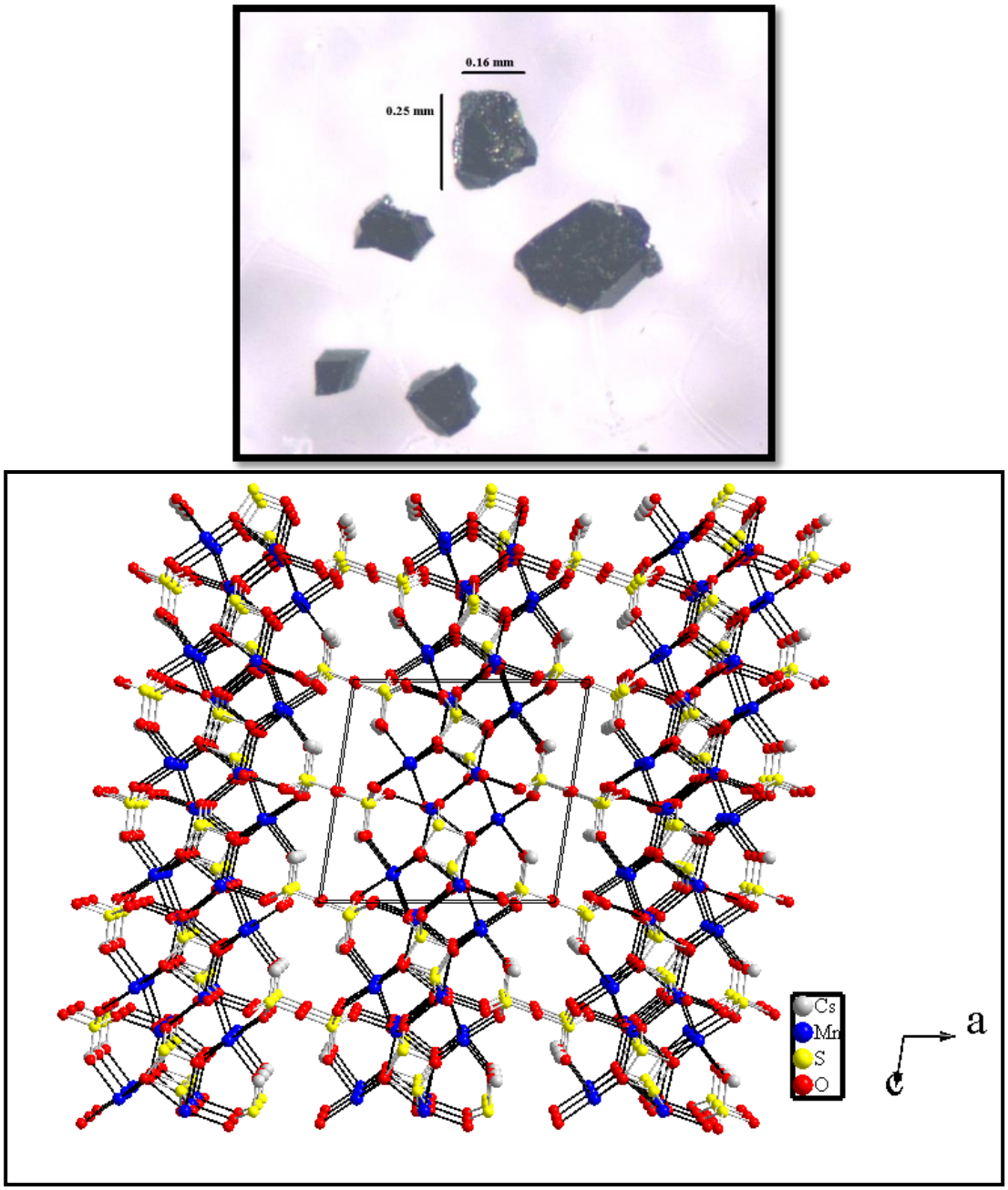


Figure 3.5: optical image showing the chunky looking morphology of the crystals of **2** (top). Perspective view of **2** showing the $[Mn_4(S_2O_7)(SO_4)_2]^{2-}$ slabs parallel along the bc plane (bottom).

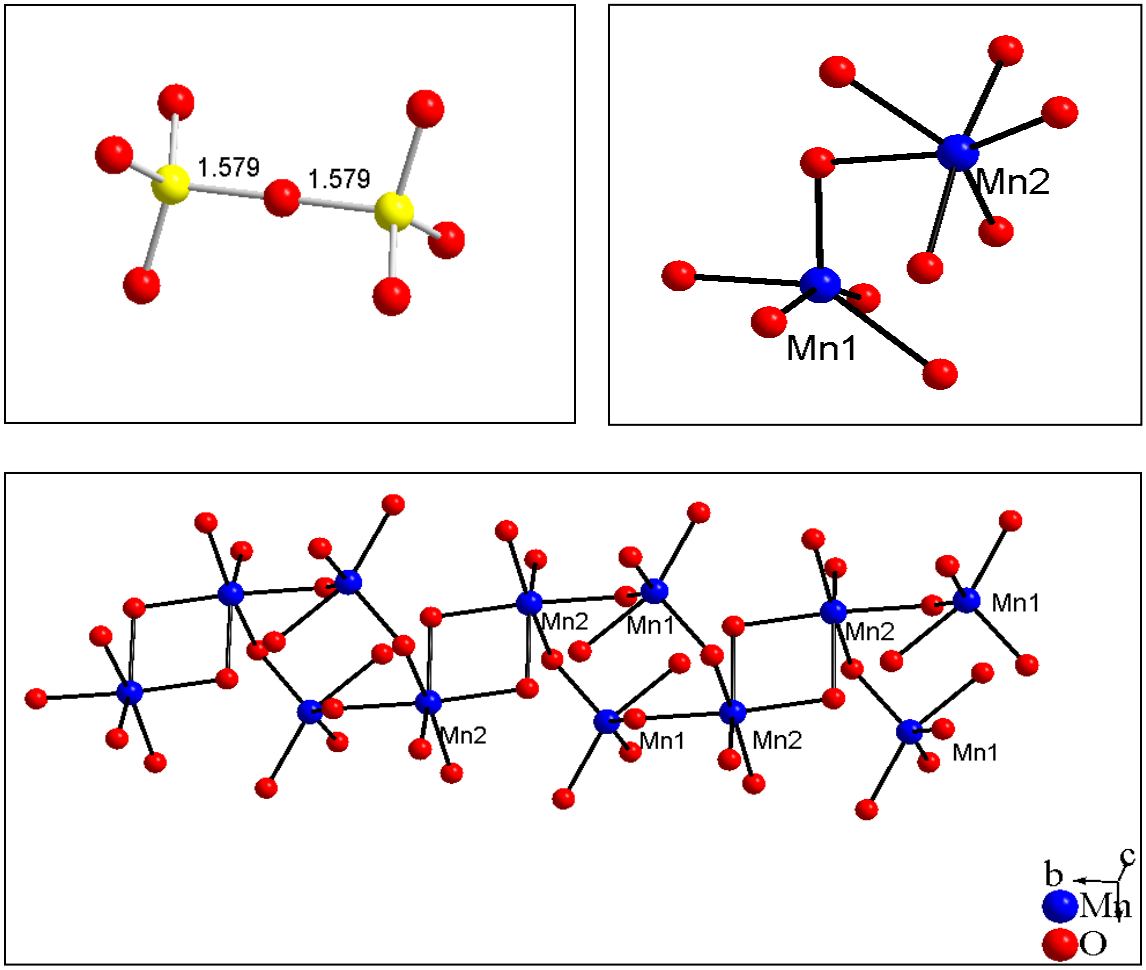


Figure 3.6: Different coordination environments for Mn1 and Mn2 (top right). The structure of the sulfate unit shows a linear ∠S-O-S with the staggered configuration (top left). The connection between Mn1 and Mn2 through the edge–shared $MnO_n$ (n = 5,6) polyhedra (bottom).

Table 3.6: Crystallographic data for $Cs_2Mn_4(S_2O_7)(SO_4)_2$ **2**

| | |
|---|---|
| Empirical formula | $Cs_2Mn_4S_4O_{15}$ |
| Formula weight (amu) | 853.81 |
| Color/shape | black chunk |
| Crystal system | Monoclinic |
| Space group, Z | $P2_1/c$ (14), 2 |
| T, °K | 293 |
| a (Å) | 10.637(2) |
| b (Å) | 6.721(13) |
| c (Å) | 10.129(2) |
| ß° | 98.96(3) |
| Cell volume $Å^3$ | 715.3(2) |
| Density, calcd ( g/cm3) | 2.661 |
| μ (Mo Kα), $mm^{-1}$ | 6.716 |
| $F_{000}$ | 503 |
| Data/restraints/parameters | 1251/0/116 |
| Final R1 / wR2[I > 2σ(I)] | 0.0242/0.0610 |
| R1/wR2 (all data) | 0.0237/0.0604 |
| GOF | 1.181 |

Table 3.7: Bond Valence Sum calculation for **2**

| **S1 -O distances** | 4+ | 6+ | **S2 - O distances** | 4+ | 6+ |
|---|---|---|---|---|---|
| 1.510 | 1.3608 | 1.4364 | 1.531 | 1.2858 | 1.3572 |
| 1.511 | 1.3564 | 1.4318 | 1.539 | 1.2583 | 1.3281 |
| 1.519 | 1.3281 | 1.4019 | 1.545 | 1.2380 | 1.3068 |
| 1.579 | 1.1296 | 1.1924 | 1.549 | 1.2247 | 1.2927 |
| | | | | | |
| **BVS** | 5.18 | 5.46 | **BVS** | 5.01 | 5.28 |

| **Mn1 -O distances** | 2+ | 3+ | **Mn2 - O distances** | 2+ | 3+ |
|---|---|---|---|---|---|
| 2.094 | 0.4397 | 0.4055 | 2.083 | 0.4530 | 0.4177 |
| 2.105 | 0.4268 | 0.3936 | 2.183 | 0.3457 | 0.3188 |
| 2.124 | 0.4055 | 0.3739 | 2.192 | 0.3374 | 0.3111 |
| 2.309 | 0.2459 | 0.2268 | 2.205 | 0.3258 | 0.3004 |
| 2.162 | 0.3659 | 0.3374 | 2.232 | 0.3028 | 0.2792 |
| | | | 2.315 | 0.2420 | 0.2231 |
| **BVS** | 1.88 | 1.74 | **BVS** | 2.01 | 1.85 |

Table 3.8: Fractional atomic coordinates and isotropic or equivalent isotropic displacement parameters ($Å^2$) for **2**

| | x | y | z | Uiso*/Ueq |
|---|---|---|---|---|
| Cs | 0.87046 (2) | 0.08285 (4) | 0.79736 (3) | 0.02110 (17) |
| Mn1 | 0.70616 (5) | −0.11778 (8) | 1.12560 (5) | 0.00851 (18) |
| Mn2 | 0.58531 (5) | 0.35288 (8) | 0.92119 (5) | 0.00734 (19) |
| S1 | 1.14079 (8) | 0.06924 (13) | 0.55227 (9) | 0.0100 (2) |
| S2 | 0.54424 (8) | −0.14311 (13) | 0.84789 (9) | 0.0086 (2) |
| O1 | 0.6109 (2) | 0.0306 (4) | 0.9297 (2) | 0.0092 (5) |
| O2 | 0.4020 (3) | −0.1055 (4) | 0.7949 (3) | 0.0105 (5) |
| O3 | 0.5546 (2) | −0.3250 (4) | 0.9423 (3) | 0.0096 (5) |
| O4 | 1.1473 (3) | 0.0908 (4) | 0.7017 (3) | 0.0173 (7) |
| O5 | 0.6057 (2) | −0.1744 (4) | 0.7225 (3) | 0.0102 (5) |
| O6 | 1.1563 (3) | 0.2624 (4) | 0.4805 (3) | 0.0189 (6) |
| O7 | 1.2219 (3) | −0.0992 (4) | 0.5114 (3) | 0.0132 (6) |
| O8 | 1 | 0 | 0.5 | 0.0345 (12) |

Table 3.9: Atomic displacement parameters (Å$^2$) for **2**

| | U11 | U22 | U33 | U12 | U13 | U23 |
|---|---|---|---|---|---|---|
| Cs | 0.0265 (2) | 0.0186 (2) | 0.0197 (2) | −0.00232 (9) | 0.00828 (13) | −0.00273 (9) |
| Mn1 | 0.0087 (3) | 0.0098 (3) | 0.0076 (3) | 0.0012 (2) | 0.0031 (2) | 0.0011 (2) |
| Mn2 | 0.0076 (3) | 0.0071 (3) | 0.0073 (3) | −0.0002 (2) | 0.0010 (2) | 0.0000 (2) |
| S1 | 0.0081 (5) | 0.0122 (5) | 0.0096 (5) | −0.0010 (3) | 0.0008 (3) | 0.0009 (3) |
| S2 | 0.0103 (5) | 0.0081 (5) | 0.0077 (4) | 0.0006 (3) | 0.0018 (3) | −0.0002 (3) |
| O1 | 0.0087 (11) | 0.0094 (12) | 0.0094 (12) | −0.0013 (10) | 0.0006 (9) | −0.0016 (10) |
| O2 | 0.0078 (12) | 0.0141 (14) | 0.0093 (13) | 0.0022 (10) | 0.0004 (10) | −0.0008 (10) |
| O3 | 0.0119 (12) | 0.0062 (12) | 0.0114 (13) | 0.0011 (9) | 0.0043 (9) | 0.0026 (10) |
| O4 | 0.0193 (15) | 0.0236 (18) | 0.0083 (14) | 0.0045 (11) | 0.0006 (11) | −0.0001 (10) |
| O5 | 0.0119 (12) | 0.0113 (14) | 0.0081 (12) | 0.0014 (10) | 0.0042 (10) | 0.0002 (10) |
| O6 | 0.0222 (14) | 0.0139 (14) | 0.0233 (15) | 0.0029 (11) | 0.0118 (12) | 0.0080 (12) |
| O7 | 0.0085 (13) | 0.0146 (14) | 0.0162 (14) | 0.0038 (10) | 0.0006 (10) | −0.0037 (11) |
| O8 | 0.0042 (19) | 0.043 (3) | 0.053 (3) | −0.006 (2) | −0.0040 (18) | −0.017 (3) |

.

Table 3.10: Selected bond distances for **2**

| Bond | distances (A) | Bond | distances (A) |
|---|---|---|---|
| Cs—O7$^{i}$ | 3.130 (3) | Mn2—O7$^{ii}$ | 2.083 (3) |
| Cs—O7$^{ii}$ | 3.143 (3) | Mn2—O1 | 2.183 (3) |
| Cs—O6$^{iii}$ | 3.160 (3) | Mn2—O3$^{vi}$i | 2.192 (3) |
| Cs—O4 | 3.240 (3) | Mn2—O3$^{ix}$ | 2.205 (3) |
| Cs—O1 | 3.270 (3) | Mn2—O2$^{v}$ | 2.232 (3) |
| Cs—O5 | 3.291 (3) | Mn2—O5$^{v}$ | 2.315 (3) |
| Cs—O4$^{iii}$ | 3.313 (3) | | |
| Cs—O4$^{ii}$ | 3.419 (3) | S1—O6 | 1.510 (3) |
| Cs—O6$^{iv}$ | 3.466 (3) | S1—O4 | 1.511 (3) |
| Cs—O8 | 3.5457 (9) | S1—O7 | 1.519 (3) |
| Cs—O2v | 3.580 (3) | S1—O8 | 1.5789(9) |
| | | | |
| Mn1—O5$^{vi}$ | 2.094 (3) | S2—O5 | 1.531 (3) |
| Mn1—O6$^{iii}$ | 2.105 (3) | S2—O1 | 1.539 (3) |
| Mn1—O2$^{vii}$ | 2.124 (3) | S2—O2 | 1.545 (3) |
| Mn1—O4$^{viii}$ | 2.162 (3) | S2—O3 | 1.546 (3) |
| Mn1—O1 | 2.309 (3) | | |

Symmetry codes: (i) −*x*+2, −*y*, −*z*+1; (ii) −*x*+2, *y*+1/2, −*z*+3/2; (iii) −*x*+2, *y*−1/2, −*z*+3/2; (iv) *x*, −*y*+1/2, *z*+1/2; (v) −*x*+1, *y*+1/2, −*z*+3/2; (vi) *x*, −*y*−1/2, *z*+1/2; (vii) −*x*+1, −*y*, −*z*+2; (viii) −*x*+2, −*y*, −*z*+2; (ix) *x*, *y*+1, *z*; (x) −*x*+1, *y*−1/2, −*z*+3/2; (xi) *x*, *y*−1, *z*; (xii) *x*, −*y*−1/2, *z*−1/2; (xiii) *x*, −*y*+1/2, *z*−1/2.

Table 3.11 : Selected bond angles for **2**

| Bond | angle$^{o}$ | Bond | angle$^{o}$ |
|---|---|---|---|
| O5$^{vi}$—Mn1—O6$^{iii}$ | 115.47 (11) | O4—S1—O7 | 113.90 (16) |
| O5$^{vi}$—Mn1—O2$^{vii}$ | 86.99 (11) | O6—S1—O8 | 105.15 (13) |
| O6$^{iii}$—Mn1—O2$^{vii}$ | 157.52 (11) | O4—S1—O8 | 104.89 (13) |
| O5$^{vi}$—Mn1—O4$^{viii}$ | 91.91 (11) | O7—S1—O8 | 103.77 (11) |
| O6$^{iii}$—Mn1—O4$^{viii}$ | 88.52 (11) | O5—S2—O1 | 109.28 (15) |
| O2$^{vii}$—Mn1—O4$^{viii}$ | 89.95 (10) | O5—S2—O2 | 104.82 (15) |
| O5$^{vi}$—Mn1—O1 | 120.22 (10) | O1—S2—O2 | 114.02 (14) |
| O6$^{iii}$—Mn1—O1 | 88.47 (11) | O5—S2—O3 | 113.97 (15) |
| O2$^{vii}$—Mn1—O1 | 80.18 (10) | O1—S2—O3 | 106.52 (14) |
| O4v$^{iii}$—Mn1—O1 | 145.44 (11) | O2—S2—O3 | 108.43 (15) |
| O7$^{ii}$—Mn2—O1 | 91.72 (10) | S2—O1—Mn2 | 133.40 (15) |
| O7$^{ii}$—Mn2—O3$^{vii}$ | 122.49 (11) | S2—O1—Mn1 | 103.80 (14) |
| O1—Mn2—O3$^{vii}$ | 89.05 (10) | Mn2—O1—Mn1 | 119.85 (11) |
| O7$^{ii}$—Mn2—O3$^{ix}$ | 88.24 (10) | S2—O2—Mn1$^{vii}$ | 122.88 (15) |
| O1—Mn2—O3$^{ix}$ | 171.83 (10) | S2—O2—Mn2$^{x}$ | 96.58 (14) |
| O3$^{vii}$—Mn2—O3$^{ix}$ | 84.10 (10) | Mn1$^{vii}$—O2—Mn2$^{x}$ | 125.40 (12) |
| O7$^{ii}$—Mn2—O2$^{v}$ | 95.48 (11) | S2—O3—Mn2$^{vii}$ | 117.88 (14) |
| O1—Mn2—O2$^{v}$ | 97.86 (10) | S2—O3—Mn2$^{xi}$ | 135.56 (15) |
| O3$^{vii}$—Mn2—O2$^{v}$ | 141.27 (10) | Mn2$^{vii}$—O3—Mn2$^{xi}$ | 95.90 (10) |
| O3$^{ix}$—Mn2—O2$^{v}$ | 90.27 (10) | S1—O4—Mn1$^{viii}$ | 137.14 (18) |
| O7$^{ii}$—Mn2—O5$^{v}$ | 160.26 (11) | S2—O5—Mn1$^{xii}$ | 142.72 (16) |
| O1—Mn2—O5$^{v}$ | 92.19 (9) | S2—O5—Mn2$^{x}$ | 93.70 (12) |
| O3$^{vii}$—Mn2—O5$^{v}$ | 76.93 (10) | Mn1$^{xii}$—O5—Mn2$^{x}$ | 102.73 (11) |
| O3$^{ix}$—Mn2—O5$^{v}$ | 90.59 (9) | S1—O6—Mn1$^{ii}$ | 135.37 (17) |
| O2$^{v}$—Mn2—O5$^{v}$ | 64.81 (10) | S1—O7—Mn2$^{iii}$ | 126.69 (16) |
| O6—S1—O4 | 114.12 (17) | S1—O8—S1i | 180 |
| O6—S1—O7 | 113.58 (16) | | |

## Conclusion

In summary, an exploratory synthesis has been made toward new polyoxometalate hybrid materials. Compound **1** contains polyoxovanadate cluster with formula $Cs_4(SO_4@V_{12}As_8O_{40})$, and compound **2** $Cs_2Mn_4(S_2O_7)(SO_4)_2$ adopts a condensed low-dimensional network structure of Mn oxides. Compounds **1** and **2** were isolated from two reactions loaded with same reactants, but different temperature programs. Compound **1** was set at 160 $^oC$ for 48h and then cooled down to room temperature over 20h and yield black crystals of $Cs_4(SO_4@V_{12}As_8O_{40})$, a new POM Kiggen structure that is insoluble in polar solvents including water. In contrast, **2** was kept at 160 $^oC$ for only 15h and then cooled down over 50h. The isolated phase was identified as $Cs_2Mn_4(S_2O_7)(SO_4)_2$ black chuck crystals. Judging from the black color, which suggests the existence of possibly itinerate electrons, physical property (such as temperature-dependent resistivity) measurements should be in order.

In both reactions, pH was treated the same level at ~3.5 and reactants were the same as well. Obviously, changing the temperature resulted in big difference in the product. It is thought that long isotherm led to decomposition of the starting material and forms the new cluster **1,** but fast cooling did not help grow larger crystals. In **2,** however, where the reaction isothermal for 15h, it is expected that the cluster is decomposed but did not reform any cluster type. It is assumed that the big advantage of slow cooling is the formation of bigger crystals than in **1**. Considering the solution acidity as another important factor in the reaction, might help toward POM synthesis without changing

heating program. It is known that acidity help formation of the metal-oxides fragments, and since the heating course is too short for cluster reformation, as we supposed, using lower pH condition might help forming the cluster again.

Literature Cited


1. Long, D.; Tsunashima, R.; Cronin, L. *Angew. Chem. Int. Ed*. **2010**, *49*, 1736 – 1758.

2. Miras, H.; Yan, J.; Long, D.; Cronin. L. *Chem. Soc. Rev.* **2012**, *41*, 7403-7430.

3. Queen, W.; West, J.; Hwu, S. Tran, T.; Halasyamani, P.; VanDerveer, D. *Chem. Commun.* . **2012,** *48, 1665–1667.*

4. Sheldrick, G. M. SHELX97. Programs for Crystal Structure Analysis (Release 97-2). University of Göttingen, GermanySheldrick, G. M. In Crystallographic Computing 3; (**1997**).

5. Sheldrick, G. M., Kruger, C., Goddard, R., Eds.; Oxford Univ. Press: London. **1985**; ,pp 175-189.

6. Sheldrick, G. M. In SHELXTL, Version 6.1 Structure Determination Software Programs.

7. Bruker. Analytical X-ray Systems Inc. Madison, WI, USA.**2001**.

8. Rhule, J.; Hill, C.; Judd, D.; Schinazi, R.; *Chem. Rev.*, **1998**, *98*, 327-357

9. Brown, I.; Altermatt, D.; *Acta Cryst.* **1985**, *B41*, 244-247

10. Queen, W.; West, J.; Hudson, J.; Hwu, S. *Inorg. Chem*. **2011**, *21*, 11064-11068

11. Shannon, R. D. *Acta Cryst.C*. **1976**, *A32*, 751-767.

12. Arichi, J.; Pereira, M.; Esteves, P.; Louis, B. *Solid State Sciences.* **2010,** 12 **,** 1866–1869

# CHAPTER FOUR

# CONCLUSION

Polyoxometalates are a novel family of metal oxide aggregates with rich structural and chemical (with respect to acid-base and redox chemistry) properties that attracted much interest in the past two decades. One of the newly emerged fields of research development is concerning the synthesis of POM-organic hybrids where POM (mostly anionic, if not all) clusters are considered as an inorganic building block. While some researches have demonstrated the versatile formation of such inorganic-organic hybrids from bottom-up approaches, our research represents the first of its kind using POM precursors as the source of inorganic anion to construct the hybrid frameworks *via* what is finally realized as self-assembly. The success of this approach is potentially critical in the future synthesis of special-framework solids by design.

In this thesis research, the hydrothermal synthesis and characterization of new POV-bpy hybrid materials have been discussed. More specifically, the targeted hybrid is based on the POV anion from a water-soluble polyoxovanadate salt. Although we failed to demonstrated the incorporation of the selected POV anion, namely $\{Cl@V_{14}As_8O_{42}\}^{5-}$, from the employed $Cs_5V_{14}As_8O_{42}Cl$ precursor, we did synthesize a new POV-bpy hybrid possibly *via* the decomposition of the POV cluster. The new compound has the chemical formula of $(H_2bpy)(Hbpy)_2(Cl@V_{15}O_{36})\cdot n(H_2O)$. The structure suggests that the new bpy-$V_{15}$ hybrid was formed based on three types of non-covalent bonding interactions.

These include hydrogen bonding between the clusters and 4,4'-bipyridine (bpy) organic likers, π-π stacking between bpy molecules, and anion-π interactions between the so-called peripheral oxygen atoms (*i.e.*, vanadyl, V=O, or terminal oxygen atoms) of the anionic cluster and aromatic ring of bpy through which the extended structure is formed in a 3D lattice. The last type of interaction, anion-π, is thought to be enticed by the protonation of 4,4'-bpy. This interaction also supports the relatively high thermal stability as shown in the TGA study where the 4,4'-bpy molecules are not thermally released until 450 $^{o}$C. This mode of linkage is extremely rare among the POM-organic solids and the interaction can be described as "POM-organic-POM" self-assembly.

In light of structural analysis, it has been realized that pre-acidifying the solution is a key step in this synthesis. Structurally, the interactions between two chemically dissimilar building units (POV anions and neutral organic molecules) are made possible through hydrogen bonding and anion-π interaction. Lowered pH level (down to ~3.5) by adding HCl in the reaction mixture entices the formation of these otherwise weak interactions. By protonating the neutral 4,4'-bipyridine molecule, the hydrogen bonding can be made through the N−H···O linkages between the nitrogen atom of 4,4'-bipyridine and the vanadyl oxygen of cluster. This protonation is essential for the formation of charge balanced molecule. Based on the Lewis acid-base concept, bpy molecule is too basic to be linked by an electron-rich cluster anion or vice versa. This explains why the reaction is only possible in the acidic media mentioned above. Also, it is consistent with the fact that the protonation occurs on bpy to form $[Hbpy]^{+}$ and $[H_2bpy]^{2+}$ cations rather than the vanadyl oxygen atoms of anionic cluster. Further, as illustrated in chapter two

and above, protonating heterocycle aromatic ring of bpy reduces the electron density of the ring making it more susceptible for the occurrence of anion–π interaction.

We also found that temperature and cooling process are crucial parameters, but we are unclear as to how they affect the product formation in terms of POV-bpy hybrid. From several reactions where the slow cooling rate (-2 $^{o}$C/h) was applied, the formation of byp-$V_{15}$ was found possible. Fast cooling prevented the formation of byp-$V_{15}$. The size of bpy-$V_{15}$ crystals, if any, was small due to shortened nucleation time and the yield of solid byproduct(s) was low. This could only suggest that the decomposition process upon which the bpy-$V_{15}$ was formed occurred during cooling. We should also point out that the $Cs_5V_{14}As_8O_{42}Cl$ solution is subject to decomposition upon being exposed to air at room temperature. Given these observations, we will study the factors that dictate the stabilities of $\{Cl@V_{14}As_8O_{42}\}^{5-}$ anions possibly in buffer solutions.

It should be pointed out that bpy-$V_{15}$ is likely a kinetic product in the reaction where the concentration of resulting cluster anions due to decomposition is probably equally, if not more, important. Hindsight suggests that keeping the pH level constant, thus using buffer solution mentioned above probably is justified in terms of keeping the protonated bpy a constant supply as well as the POM cluster from decomposing during the course of self-assembly. Future studies should also include the investigation of chemical and physical properties of the newly discovered phases, especially from the magnetic point of view to probe any unusual phenomena due to confined magnetic spins. Last, but not least, it is worth to reinvestigate the reactions from which compounds were isolated and which, as stated in the appendix, have unsolved crystal structures table 4.1.

Completing their structures allows us to better understand the structure and bonding of self-assembled products for the future synthesis of POM-based hybrid solids potentially by design.

# APPENDIX

Table A.1: Unsolved crystal structures from unsuccessful synthesis of POM-hybrid.

| **Formula sum** | $V_{15}O_{36}Cl$ (bipy)$_3$ **A1** | $H_2$(bpy)$_3$ ($V_{14}As_8O_{42}Cl$). ($H_2O$)$_2$ **A2** | $V_{12}O_{40}As_8Cl$ [($C_4H_9$)$_4$N)]$_2$ **A3** |
|---|---|---|---|
| **Formula weight (amu)** | 1843.5 | 2523.8 | 2115.4 |
| **color/shape** | green column | black column | green rhombus |
| **Crystal system** | monoclinic | monoclinic | monoclinic |
| **Space group, Z** | $P2_1/c$ (no. 14), 4 | $C2/c$ (no. 15), 4 | $P2_1/c$ (no. 14), 4 |
| **T, °C** | 25 | 25 | 25 |
| **a (Å)** | 16.621(3) | 27.455(6) | 11.586(2) |
| **b (Å)** | 12.632(3) | 15.683(3) | 14.423(3) |
| **c (Å)** | 29.273(6) | 20.755(4 | 27.603(6) |
| **ß °** | 91.53(3) | 127.13(3) | 95.82(3) |
| **Cell volume Å$^3$** | 6143.86(200) | 7124.88(200) | 4588.8(16) |
| **Density, calcd(g/cm$^3$)** | 2.75 | 2.316 | 4.488 |
| **data/parameters** | 10805/793 | 6311/474 | 7954/367 |
| **Final R1 / wR2[I > 2σ(I)]** | 0.126/2742 | 0.1138/03062 | 0.1872/0.4389 |
| **R1/wR2 (all data)** | 0.1752/0.3182 | 0.1314/0.3267 | 0.2367/0.5220 |
| **GOF** | 1.4 | 2.2 | 1.7 |

Reaction conditions: **A1 and A2:** kept at 160 $^o$C for 48 h, cooled down to RT over 20 h, pH ~4. **A3:** kept at 160 $^o$C for 15h, cooled down to RT over 60 h. pH ~3.5.

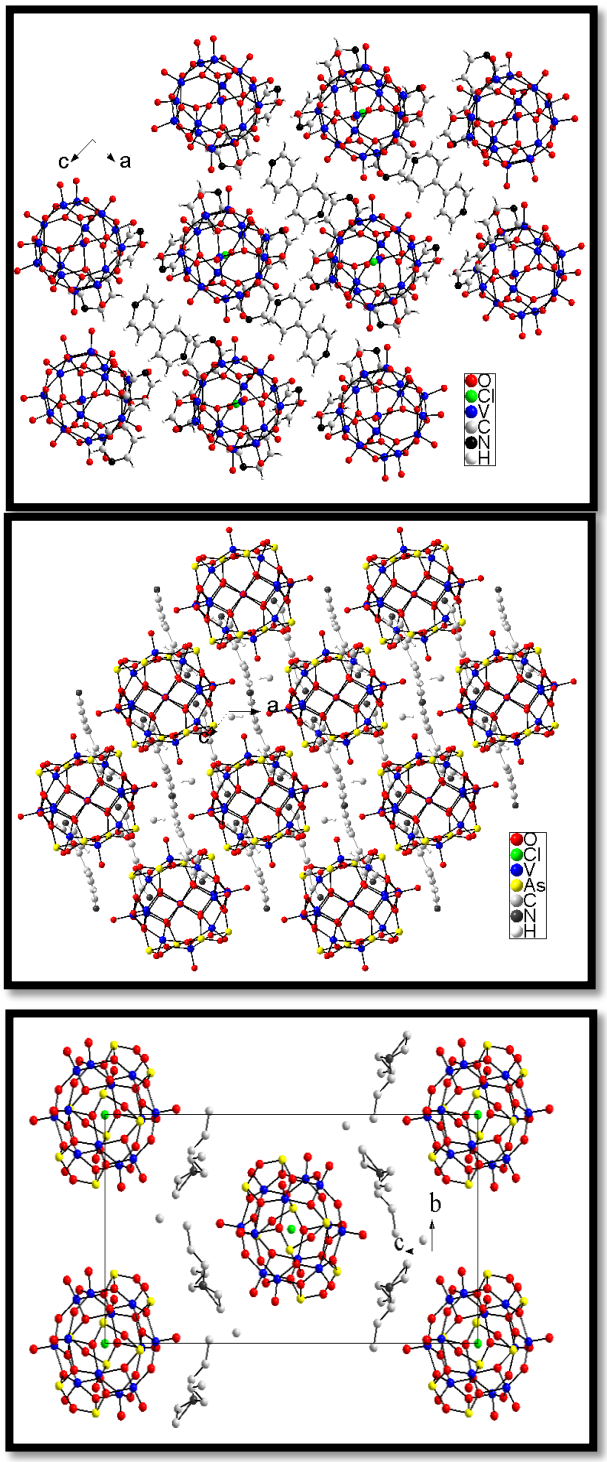


Figure A.1 : Unsolved crystal structures of , $V_{15}O_{36}Cl\ (bipy)_3$ (top), $H_2(bpy)_3\ (V_{14}\ As_8O_{42}Cl)\ (H_2O)_2$ (middle) and $V_{12}O_{40}As_8Cl\ [(C_4H_9)_4N)]_2$ (bottom).